



## Origin of $^{87}\text{Sr}$ enrichment in calcite cements in Jurassic limestones (Eastern Paris Basin, France)

Thomas Blaise, Michel Cathelineau, Philippe Boulvais, Isabelle Techer, Marie-Christine Boiron, Alexandre Tarantola, Benjamin Brigaud, Philippe Landrein

### ► To cite this version:

Thomas Blaise, Michel Cathelineau, Philippe Boulvais, Isabelle Techer, Marie-Christine Boiron, et al.. Origin of  $^{87}\text{Sr}$  enrichment in calcite cements in Jurassic limestones (Eastern Paris Basin, France). Applied Geochemistry, 2022, 136, pp.105131. 10.1016/j.apgeochem.2021.105131 . insu-03418643

**HAL Id: insu-03418643**

**<https://insu.hal.science/insu-03418643>**

Submitted on 8 Nov 2021

**HAL** is a multi-disciplinary open access archive for the deposit and dissemination of scientific research documents, whether they are published or not. The documents may come from teaching and research institutions in France or abroad, or from public or private research centers.

L'archive ouverte pluridisciplinaire **HAL**, est destinée au dépôt et à la diffusion de documents scientifiques de niveau recherche, publiés ou non, émanant des établissements d'enseignement et de recherche français ou étrangers, des laboratoires publics ou privés.

Origin of  $^{87}\text{Sr}$  enrichment in calcite cements in Jurassic limestones (Eastern Paris Basin, France)

Thomas Blaise, Michel Cathelineau, Philippe Boulvais, Isabelle Techer, Marie-Christine Boiron, Alexandre Tarantola, Benjamin Brigaud, Philippe Landrein

PII: S0883-2927(21)00262-6

DOI: <https://doi.org/10.1016/j.apgeochem.2021.105131>

Reference: AG 105131

To appear in: *Applied Geochemistry*

Received Date: 17 May 2021

Revised Date: 7 October 2021

Accepted Date: 28 October 2021

Please cite this article as: Blaise, T., Cathelineau, M., Boulvais, P., Techer, I., Boiron, M.-C., Tarantola, A., Brigaud, B., Landrein, P., Origin of  $^{87}\text{Sr}$  enrichment in calcite cements in Jurassic limestones (Eastern Paris Basin, France), *Applied Geochemistry* (2021), doi: <https://doi.org/10.1016/j.apgeochem.2021.105131>.

This is a PDF file of an article that has undergone enhancements after acceptance, such as the addition of a cover page and metadata, and formatting for readability, but it is not yet the definitive version of record. This version will undergo additional copyediting, typesetting and review before it is published in its final form, but we are providing this version to give early visibility of the article. Please note that, during the production process, errors may be discovered which could affect the content, and all legal disclaimers that apply to the journal pertain.

© 2021 Published by Elsevier Ltd.



# Origin of $^{87}\text{Sr}$ enrichment in calcite cements in Jurassic limestones (Eastern Paris Basin, France)

Thomas BLAISE<sup>1,\*</sup>, Michel CATHELINEAU<sup>2</sup>, Philippe BOULVAIS<sup>3</sup>, Isabelle TECHER<sup>4</sup>, Marie-Christine BOIRON<sup>2</sup>, Alexandre TARANTOLA<sup>2</sup>, Benjamin BRIGAUD<sup>1</sup>, Philippe LANDREIN<sup>5</sup>

<sup>1</sup> Université Paris-Saclay, CNRS, GEOPS, 91405, Orsay, France

<sup>2</sup> Université de Lorraine, CNRS, GeoRessources, 54500 Nancy, France

<sup>3</sup> Géosciences Rennes, CNRS, Univ Rennes, UMR 6118, F-35000, Rennes, France

<sup>4</sup> EA 7352 CHROME, Université de Nîmes, rue du Dr. Georges Salan, 30021 Nîmes, France

<sup>5</sup> Agence Nationale pour La Gestion des Déchets Radioactifs (ANDRA), Centre de Meuse/Haute-Marne, RD 960, 55290 Bure, France

\* Corresponding author: thomas.blaise@universite-paris-saclay.fr

## Highlights

- $^{87}\text{Sr}/^{86}\text{Sr}$  records the input of basinal allochthonous fluids through the fracture network in the Jurassic limestones
- The strontium isotope shift between the authigenic calcite and the host limestones depends on the dilution rate of radiogenic allochthonous fluids by the limestone porewaters.
- Paleo-water flows strongly modified the primary  $\delta^{18}\text{O}$  and  $^{87}\text{Sr}/^{86}\text{Sr}$  composition in bulk limestones.

## Abstract

In this contribution, the origin of fluids having cemented the Jurassic limestones in the eastern part of the Paris Basin is discussed through the isotopic composition ( $\delta^{18}\text{O}$ ,  $\delta^{13}\text{C}$ ,  $^{87}\text{Sr}/^{86}\text{Sr}$ ) of authigenic calcite crystals filling vugs and fractures. The Upper and Middle Jurassic limestones, overlying and underlying the Callovian-Oxfordian claystones, experienced dissolution and crystallization leading to a succession of calcite cements depleted in  $^{18}\text{O}$  and enriched in  $^{87}\text{Sr}$  compared to the bulk host limestone isotope composition. These isotopic shifts originate from the flow of allochthonous basinal fluids through the fracture network that developed during the main tectonic deformation events. Mixing between the allochthonous fluids and the autochthonous local porewaters is attested by variable  $^{87}\text{Sr}/^{86}\text{Sr}$  in diagenetic calcite.  $^{87}\text{Sr}$ -enriched fluids that precipitated calcite cements strongly impact the  $^{87}\text{Sr}/^{86}\text{Sr}$  ratio of present-day groundwaters in Jurassic limestones and may have modified the Callovian-Oxfordian porewater isotope composition.

## Keywords

Paris Basin, Jurassic limestones, calcite cement, strontium isotope composition, diagenesis

## Introduction

Shallow-buried carbonate rocks have received much attention over the last years, as potential reservoirs for underground water resources are becoming more and more exploited in the context of global climate change (Chen et al., 2018; Goldscheider et al., 2020). Besides, groundwaters in limestones can be extracted to produce geothermal energy (e.g., Montanari et al., 2017) or used to sequester CO<sub>2</sub> (Thibeau et al., 2009).

The petrophysical properties of limestones show considerable variations depending on depositional environments and the nature of diagenetic alterations. Commonly, carbonate cement precipitating from burial or tectonic-induced pressure-solution occludes pores, hence decreasing the reservoir capacities. When preserved, the chemical and isotopic compositions of authigenic carbonates provide information regarding the nature, origin, and timing of mineralizing fluid flows (Mangenot et al., 2018; Beaudoin et al., 2020). Such information is required in the geological characterization of underground nuclear waste storage (Mazurek, 1999; Blyth et al., 2000; Sandström and Tullborg, 2009; Dublyansky and Spötl, 2010; de Haller et al., 2011; Drake et al., 2012; Wallin and Peterman, 2015; Drake et al., 2020). The geochemistry of calcite cements also helps to unravel tectonic evolution (André et al., 2010), and in certain cases, to date brittle deformation (Goodfellow et al., 2017; Pagel et al., 2018; Mazurek et al., 2018; Sutcliffe et al., 2020; Davis et al., 2020). Finally, it may help understand the geometry and hydrologic properties of present-day aquifers (Carpentier et al., 2015; Brigaud et al., 2009a).

The strontium isotope composition of authigenic calcite is of primary interest in discussing fluid-rock interactions and unravelling fluid pathways. Early diagenetic marine cements commonly record the <sup>87</sup>Sr/<sup>86</sup>Sr values of contemporaneous seawater (Brigaud et al., 2009a; Lerouge et al., 2010; Swart, 2015). During meso-telogenesis, low fluid/rock ratios and extensive dissolution-recrystallization may result in calcite cements having a Sr isotope composition similar to the adjacent host rocks (Barker et al., 2009). However, it is frequent that calcite cements show <sup>87</sup>Sr depletion or enrichment compared to the host marine carbonate rocks (Worden and Matray, 1995). Such isotopic shift may originate from multiple factors, including the fluid source and the origin of dissolved Sr (Brand et al., 2010), its interaction with soils or rocks and the fluid-rock ratio during calcite precipitation or recrystallization (Banner, 1995). Deciphering the contribution of these parameters requires coupling the <sup>87</sup>Sr/<sup>86</sup>Sr ratios with other information such as the stable oxygen and carbon isotope compositions to reconstruct the diagenetic evolution of carbonate rocks (Swart, 2015; Paganoni et al., 2019; Debenham et al., 2020; Erhardt et al., 2020).

In the eastern Paris Basin, the Oxfordian to Kimmeridgian (Upper Jurassic Limestones, UJL) and Bathonian to Bajocian (Middle Jurassic Limestones, MJL) carbonate platforms have been intensively cemented, despite shallow burial (< 1000 m, Blaise et al., 2014). These limestone units are separated by a 150 m thick succession of Callovian-Oxfordian claystones. The latter is currently under investigation by the French national radioactive waste management agency (Andra) for the storage of nuclear wastes. The porosity in the Jurassic limestones is now largely plugged by a series of calcite cements, which have been thoroughly characterized over the last fifteen years (Buschaert et al., 2004; Vincent et al., 2007; Brigaud et al., 2009a; André et al., 2010; Lavastre et al., 2011; Carpentier et al., 2014). A paragenetic sequence of these cements

was proposed by Carpentier et al. (2014), leading to a conceptual diagenetic model, however, not integrating the Sr isotope composition information. While the Sr isotope composition of present-day groundwaters in the Jurassic limestones is homogeneous, a few previous studies have reported variable  $^{87}\text{Sr}/^{86}\text{Sr}$  enrichment in authigenic calcite compared to the adjacent host rocks (Maes, 2002; Brigaud et al., 2009a). The origin of high  $^{87}\text{Sr}/^{86}\text{Sr}$  ratios in paleo-fluids remains poorly explored. Moreover, the origin of the calcite-mineralizing fluids is still discussed. Brigaud et al. (2020) evidenced elevated crystallization temperatures, up to 110 °C, from the  $\Delta_{47}$  clumped isotope composition of calcite cements in the MJL, suggesting the flow of hydrothermal waters along the major regional faults.

In this contribution, the underexplored Sr isotope composition of calcite cements was studied and used to discuss the contribution of basinal allochthonous fluids in the crystallization of calcite cements, and potential connections between aquifers along deeply-rooted faults. The possible sources leading to high  $^{87}\text{Sr}/^{86}\text{Sr}$  values recorded in authigenic calcite are examined in terms of fluid provenance, fluxes, mixing and fluid-rock ratios. These new data are compiled with other published isotopic dataset and compared with the  $^{87}\text{Sr}/^{86}\text{Sr}$  values reported by Lerouge et al. (2010) for the detrital and authigenic mineral components in the Callovian-Oxfordian claystones. A possible transfer of strontium by advective flow and diffusion throughout the Jurassic section is mainly discussed as it can be an excellent marker of system openness.

## **Geological setting and diagenetic framework**

In the eastern Paris Basin, the Lower Jurassic formations consist mainly of marls and shales deposited during the Carnian to the Toarcian stratigraphic cycle (Guillocheau et al., 2000, Landrein et al., 2013). The Early Bajocian marked the transition to a vast carbonate environment, with the deposition of oobioclastic sediments together with coral buildups (Brigaud et al., 2014). A significant facies change occurred at the Early/Late Bajocian transition, with mixed carbonate (ooid-dominated) and siliciclastic sedimentation (Brigaud et al., 2009b). A new carbonate ramp then developed in the northeastern Paris Basin during the Bathonian. A general drowning of the platform resulting in the deposition of clay-rich sediments started during the Callovian and lasted until the Early Oxfordian. The depositional environment gradually gets back to carbonate sedimentation during the Middle Oxfordian, with reefal-dominated and oolitic limestones. A major carbonate production crisis occurred at the Oxfordian/Kimmeridgian transition (Lefort et al., 2011), with marls-dominated sedimentation, coming next with a mixed carbonate and siliciclastic ramp environment during the Tithonian. During the Early Cretaceous, an extended emersion is recorded in the Paris Basin, associated with erosion and the karstification of the carbonate substrate (e.g., the Upper Jurassic Limestones in the studied area). A significant transgression occurred in Late Cretaceous times resulting in chalk deposition, which thickness reached 300 to 400 m in the study area (Blaise et al., 2014). The eastern basin margin definitively emerged and experienced weathering and erosion during the Cenozoic, allowing the progressive exhumation of the underlying Jurassic and Triassic sediments, which presently crop out in the study area.

During the Late Cretaceous to the Cenozoic periods, a series of compressional deformation events related to the Pyrenean and Alpine orogenies affected this part of the Basin (André et al.,

121 2010, Pisapia et al., 2018). Also, an extensional deformation synchronous to the formation of  
122 the Rhine graben occurred during the Oligocene period. The Gondrecourt graben, which  
123 delimits the Andra Underground Research Laboratory (URL) area (Figure 1) formed at that time.  
124



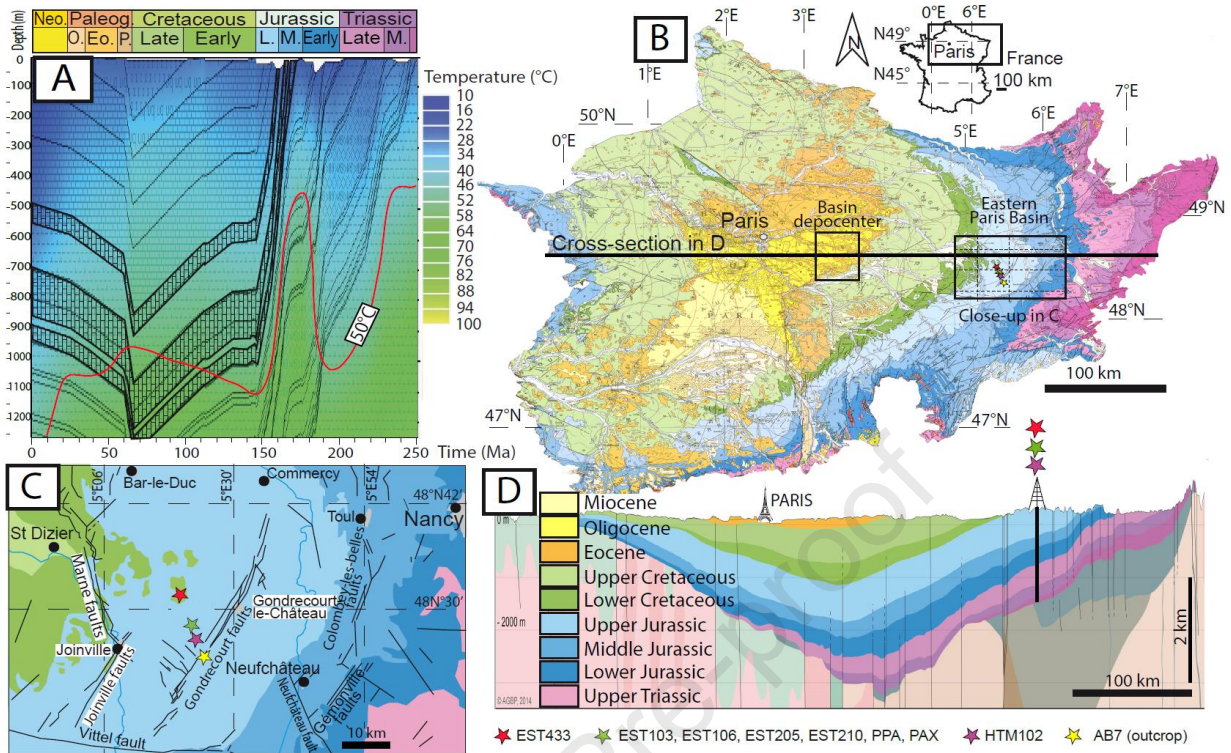


Figure 1. A- Thermal and depth evolution through time of the Jurassic and Cretaceous rocks in the eastern Paris Basin. The Middle (MJL) and Upper Jurassic limestones (UJL) are indicated, together with the 50 °C isotherm (modified from Blaise et al., 2014). B- Geological map of the Paris Basin and location of the study area. C- Detailed map of the study area with faults and wells locations. D- Geological cross-section from Gély and Hanot (2014), with the location of wells.

The diagenetic sequence in Jurassic limestones in the eastern Paris Basin was synthesized by Carpentier et al. (2014). These authors identified four successive calcite cement generations (Table 1).

Cement	Cathodoluminescence	Chemistry	$\delta^{18}\text{O}$	Abundance	Presumed age	U-Pb age
Cal1	Bright Orange	Non-ferroan	-3.5 to -6.0	0 % in UJL 35 % in MJL	Late Jurassic - Early Cretaceous	147.8 ± 3.8 Ma [1] 147.7 ± 4.7 Ma [2]
Cal2	Dull Brown	Ferroan	-6.7 to -8.1	highly variable in UJL 35 % in MJL	Early - Late Cretaceous	161 ± 8.6 Ma [2] 157.7 ± 7.7 Ma [2]
Cal3	Bright Orange	Non-ferroan	-7.8 to -9.7	up to 50 % in UJL 0 - 15 % in MJL	Late Cretaceous - Paleogene	33.5 ± 2.8 Ma [1] 41.5 ± 4.8 Ma [2] 34.9 ± 1.2 Ma [3] 43 ± 1 Ma [3]
Cal4	Dull Brown	Non-ferroan	-8.1 to -11.9	highly variable, up to 90 % in UJL 0 - 10 % in MJL	Neogene	Unknown

Table 1. Synthetic table summarizing the characteristics of calcite cements in Jurassic limestones. Petro-geochemical features of calcite cements are from Carpentier et al. (2014). UJL: Upper Jurassic limestones. MJL: Middle Jurassic limestones. Geochronological data are

from [1] Pisapia et al., 2017. [2] Brigaud et al., 2020. [3] Pagel et al., 2018. U-Pb ages of Cal1 and Cal2 are determined in Bathonian and Bajocian Formations, respectively.

## Sampling strategy

Figure 1 provides sample localities, and sampling depths on drill cores are summarized in Figure 2. Core samples are coming from wells drilled in the vicinity of the Andra URL. Wells PPA, PAX, EST205, EST210, and EST103 are located a few hundred meters from each other. Well HTM102 is located 2 km south-east of these wells, and well EST433, 8 km north-west.

Twenty-nine core samples were collected in wells PPA (3 samples), PAX (2 samples), EST205 (4 samples), and EST433 (20 samples). Data coming from these new samples were integrated into a database created from the compilation of previously published data, which include:

- 42 analyses from wells HTM102 (37 samples) and EST103 (5 samples) from Buschaert et al. (2004) for stable O and C isotope composition and from Maes (2002) for Sr isotope composition,
- 23 samples from EST210 from Hibschi et al. (2005) for O, C and Sr isotope compositions,
- 5 samples from HTM102 (2 samples) and EST210 (3 samples) from Brigaud et al. (2009) for O, C and Sr isotope compositions.

Calcite cements consist of pure calcite from fractures or vugs in the Jurassic limestones. In some cases, due to too small crystals, strontium, oxygen and carbon isotope compositions could not have been measured from a single crystal. When possible, the O, C, and Sr isotope compositions of the bulk limestone were also measured by sampling a fragment at the vicinity of vugs and fractures.

To discuss the lateral extent of fluid flows involved in calcite precipitation, we have analyzed 5 calcite samples crosscutting the upper Oxfordian to Lower Kimmeridgian limestones, at the eastern flank of the Gondrecourt graben ("AB7" samples, Augeville locality, Figure 1). These calcite fill fractures and hydraulic breccias dated by U-Pb geochronology at  $34.9 \pm 1.2$  Ma and  $43.0 \pm 1.0$  Ma, respectively (Pagel et al., 2018).

In this paper, "vug-filling" and "fracture-filling" calcite are discriminated. Based on petrography and oxygen isotopic composition, authigenic calcite can be classified as follows:

- Calcite filling vug and fracture corresponding to Cal3 and Cal4 in the MJL and UJL, and with  $\delta^{18}\text{O} < -7.7$  ‰V-PDB
- Calcite with  $\delta^{18}\text{O} > -7.7$  ‰V-PDB corresponding to Cal1 and Cal2 in the MJL typical of the vug-filling samples.



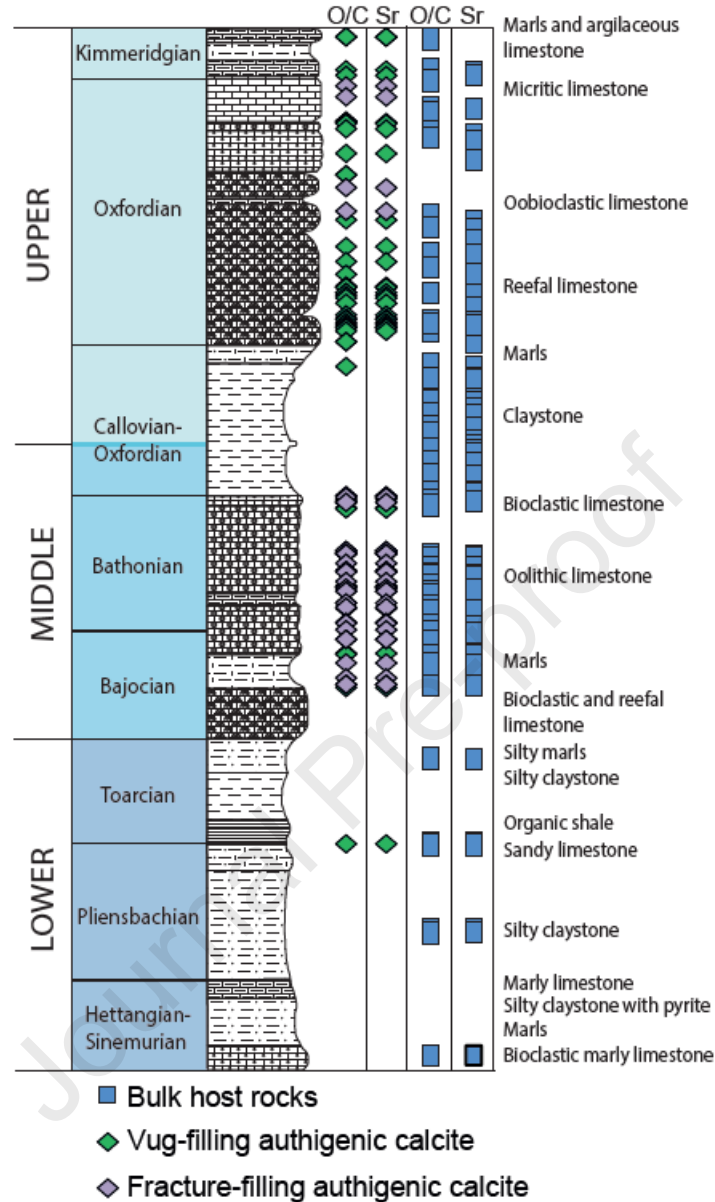


Figure 2. Graphical representation of all core samples considered for this study, including those coming from previous publications. Depths were normalized to the HTM102 borehole (see text for details).

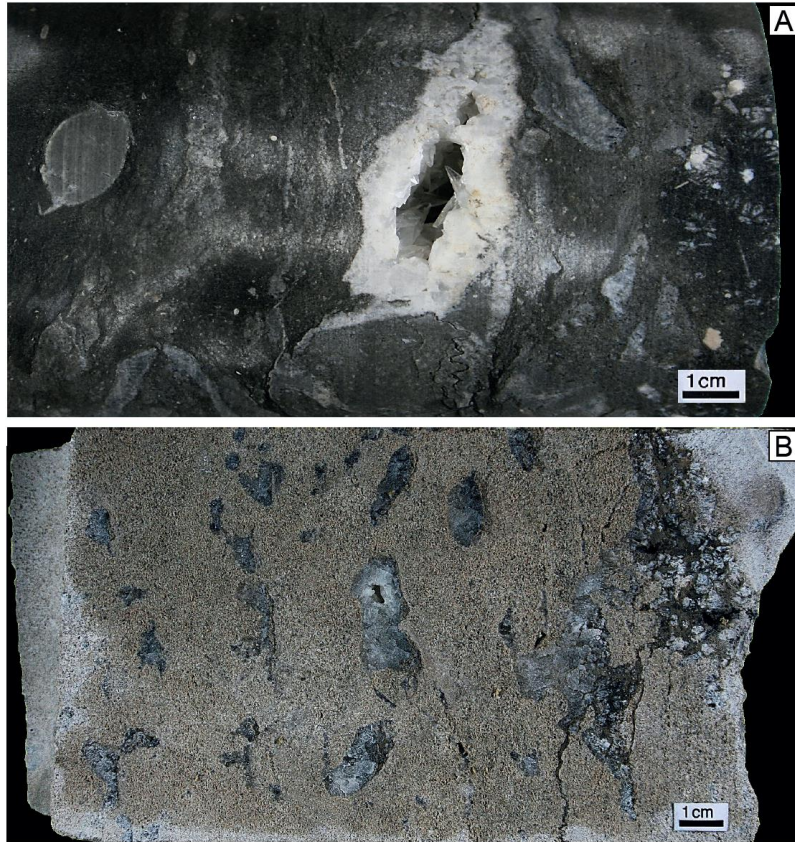
### Analytical procedures

Polished thin sections (30  $\mu\text{m}$ ) were prepared for petrographic observations under optical and cathodoluminescence microscopy. Calcite crystals were extracted from fractures and vugs and picked out under the microscope to select monogenic crystals from cores (Figure 3). Calcite fragments at the vicinity of the host rocks were excluded to avoid contamination. Fragments of the host limestones were extracted at the vicinity of fractures and vugs. For Sr isotope measurements, limpid calcite cements and host rocks were dissolved in 1N  $\text{HNO}_3$  at room

temperature for 5 minutes. Samples of bulk marls and shales from underlying Liassic units (Toarcian to Hettangian) were also included to investigate upward Sr transfers. Separation of Sr was conducted on a Sr-resin, following the methodology described by Pin et al. (2003). Leachates were evaporated, redissolved in HNO<sub>3</sub>, and deposited on Ta filaments. Sr isotopes were measured on a Triton TI TIMS at the GIS laboratory (Nîmes, France). Values are reported as <sup>87</sup>Sr/<sup>86</sup>Sr ratios. The external reproducibility of the isotopic measurements was controlled by periodic analysis of the NBS 987 standard, providing a mean <sup>87</sup>Sr/<sup>86</sup>Sr ratio of  $0.710258 \pm 2.10^{-6}$  (2 $\sigma$ ). The <sup>87</sup>Sr/<sup>86</sup>Sr ratios were measured at least 90 times to ensure an analytical error below  $5.10^{-6}$  (2 $\sigma$ ). For O and C isotope measurements, monogenic crystals filling vugs and fractures, together with fragments of host limestones were powdered and reacted with anhydrous H<sub>3</sub>PO<sub>4</sub> at 50 °C for 15 h. Isotopic analyses were carried out on CO<sub>2</sub> gas using a VG SIRA 10 mass spectrometer at Geosciences Rennes laboratory (France) and expressed with the conventional delta notation vs V-PDB. Analytical precision was quantified at  $\pm 0.1$  ‰ for both C and O, using in-house carbonate standard Prolabo Rennes and NBS 19 reference material.

To evaluate potential inclusions of K-bearing minerals, four calcite cement and four bulk limestone samples were dissolved and analyzed by Inductively Coupled Plasma - Optical Emission Spectrometry (ICP-OES) at the CRPG laboratory (Nancy, France) (Supplementary data).

All sample depths were normalized to the reference depth measured in the HTM102 well, using detailed lithological descriptions along well logs and previous stratigraphic correlations (Ferry et al., 2007; Brigaud et al., 2009b). This normalization facilitates the presentation and discussion of data acquired from different boreholes. This representation may induce uncertainty in the depth estimate of samples. As this uncertainty does not exceed a few meters, it does not impact the discussion and conclusions.



214

215 Figure 3. Examples of core samples with vug-filling calcite. A- Well EST205, 326 m depth. B-  
216 Well EST433, 490 m depth.

## 217 Results

### 218 Petrographic description of calcite cements

219 Petrographic characteristics of successive calcite cements are presented in Carpentier et al.  
220 (2014). Calcite cements filling vugs and fractures show homogenous textures and sometimes  
221 zoning pattern under cathodoluminescence (Figure 4D). Crystals may contain solid inclusions of  
222 the host rocks in the first crystallization stages but are limpid towards the centre or vugs and  
223 fractures. When present, eogenetic calcite cements (Figure 4C) and other early cements such  
224 as chalcedony and dolomite (Figure 4A) were excluded from sampling.



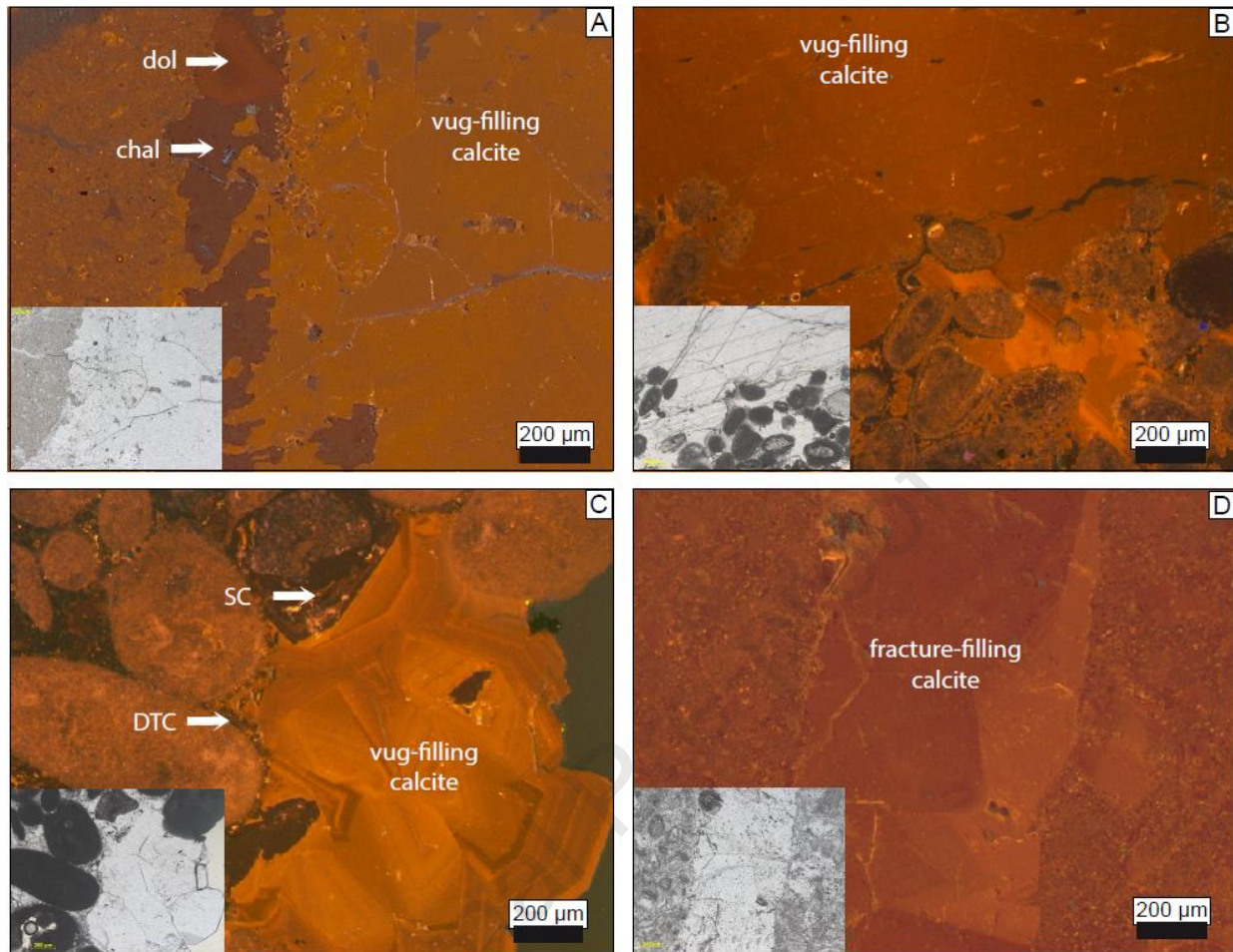


Figure 4. Photomicrographs under cathodoluminescence microscopy. Corresponding areas observed in optical microscopy are illustrated in bottom left of each photomicrograph. A- Vug-filling calcite in the Middle Oxfordian limestones (Well EST205, 330 m depth) exhibiting homogeneous cathodoluminescence without zoning. Calcite postdates dolomite (dol) and chalcedony (chal). B- Vug-filling calcite in a Bathonian grainstone (Well EST433, 490 m depth) showing similar petrographic features as the one illustrated in Figure 3A. C- Vug-filling calcite in a Bathonian grainstone (Well EST433, 495 m depth) showing a globular texture and bright orange cathodoluminescence with concentric zoning. It postdates isopachous dogtooth cements (DTC) and syntaxial cements (SC). D- Fracture-filling calcite in the Bajocian limestones (Well EST433, 660 m depth) showing zoning pattern.

#### Sr isotope composition of calcite cements

The strontium isotope ratios of bulk rocks in core samples range from 0.707162 to 0.707307 (Table 2). The authigenic calcite values range from 0.707166 to 0.707353 in the UJL and from 0.707152 to 0.707380 in the MJL (Table 3). The vugs and fractures usually yield  $^{87}\text{Sr}/^{86}\text{Sr}$  values higher than adjacent host rock. All Sr isotope data from core samples are plotted as a function of depth in Figure 5. The  $^{87}\text{Sr}/^{86}\text{Sr}$  values of calcite fracture-infilling in outcrop samples

range from 0.707309 to 0.707921 (Table 5), higher than bulk host rock values determined on two samples and yielding values of 0.707114 and 0.707157 (Table 4).

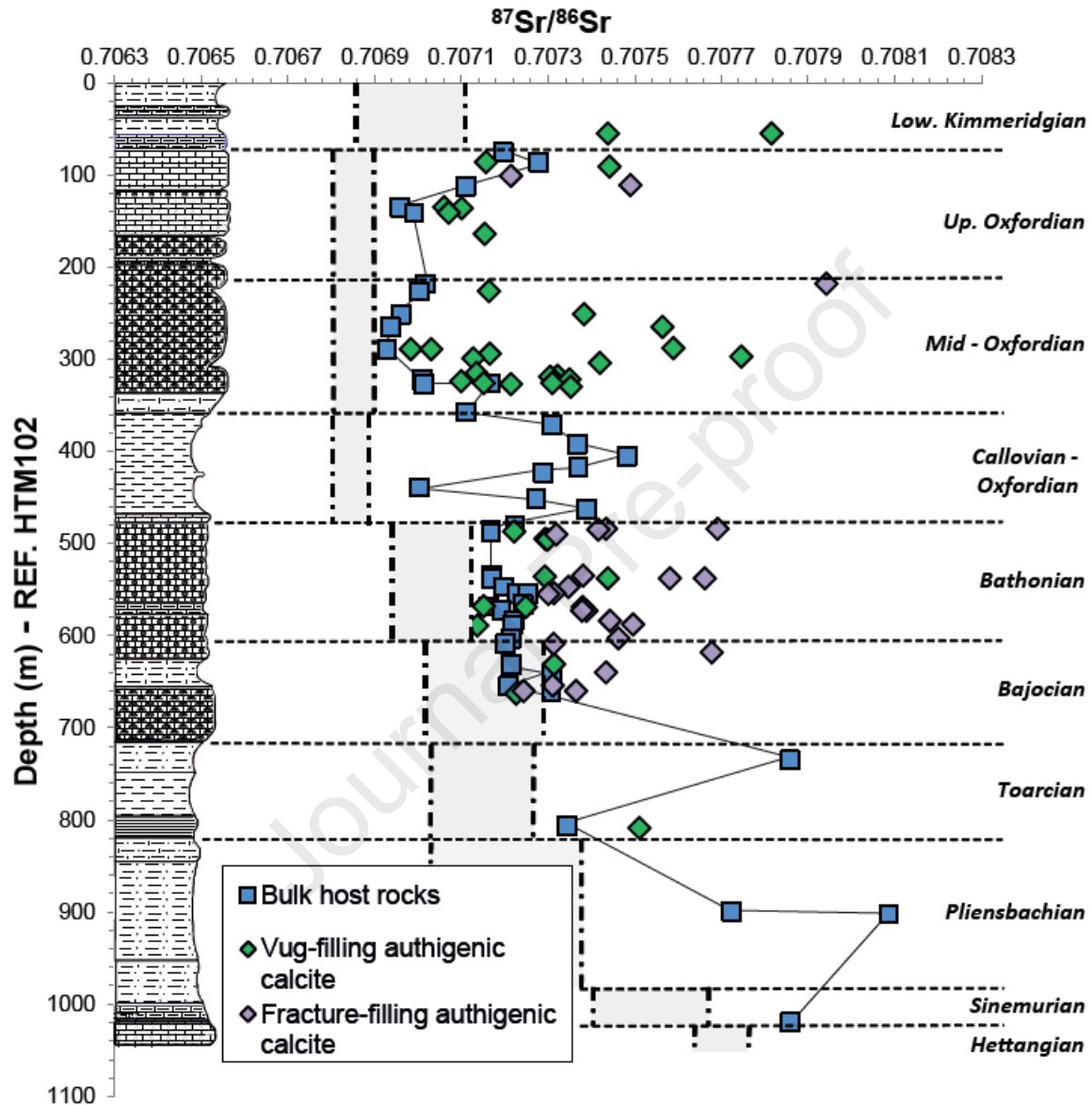
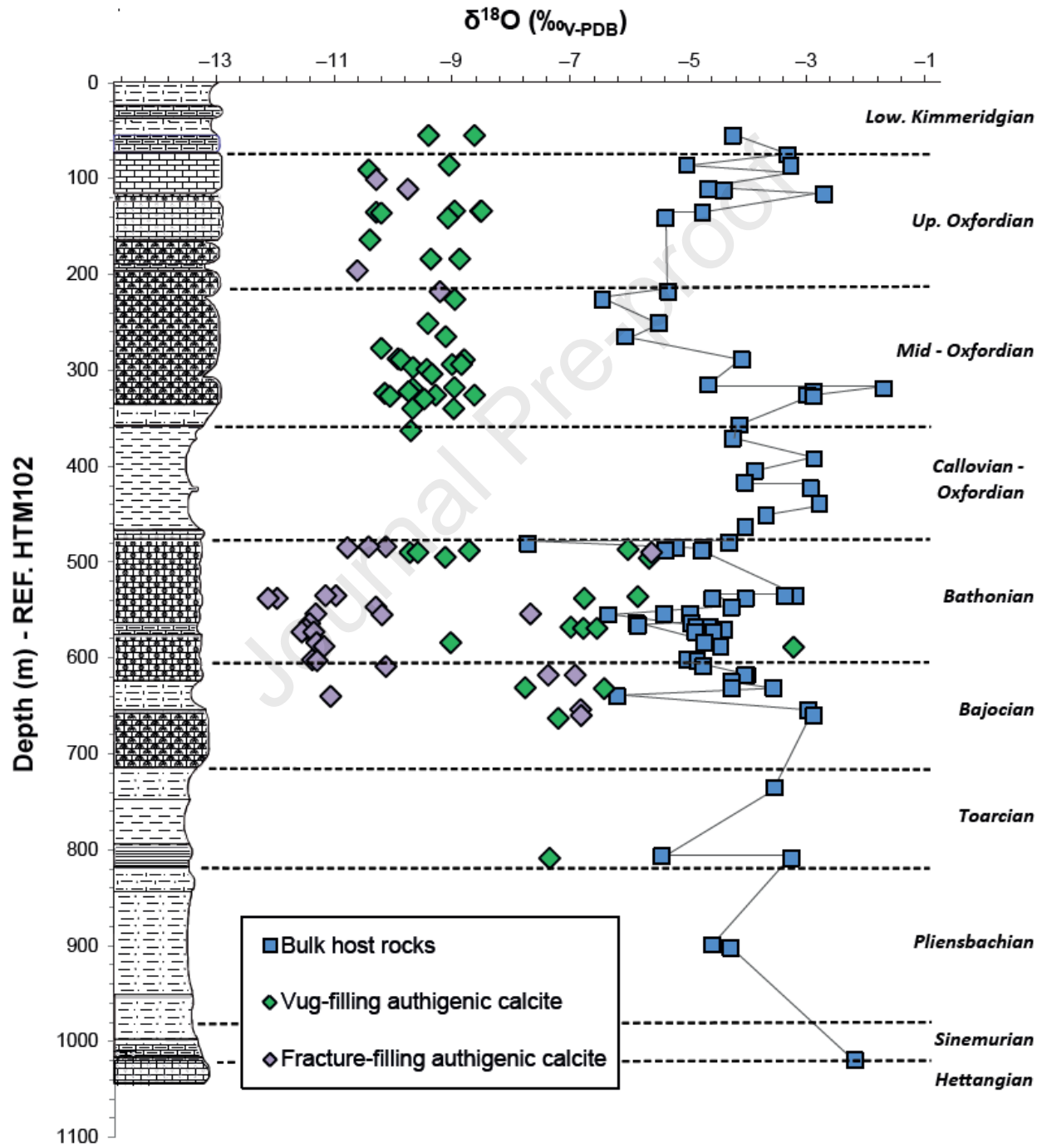


Figure 5. Vertical distribution of calcite  $^{87}\text{Sr}/^{86}\text{Sr}$  values in authigenic infillings (vugs and fractures) and in bulk limestones or marls. The depth scale of the well HTM102 is used as a reference. The average seawater values, illustrated by dashed-line grey boxes, are from Jones et al. (1994a, 1994b).

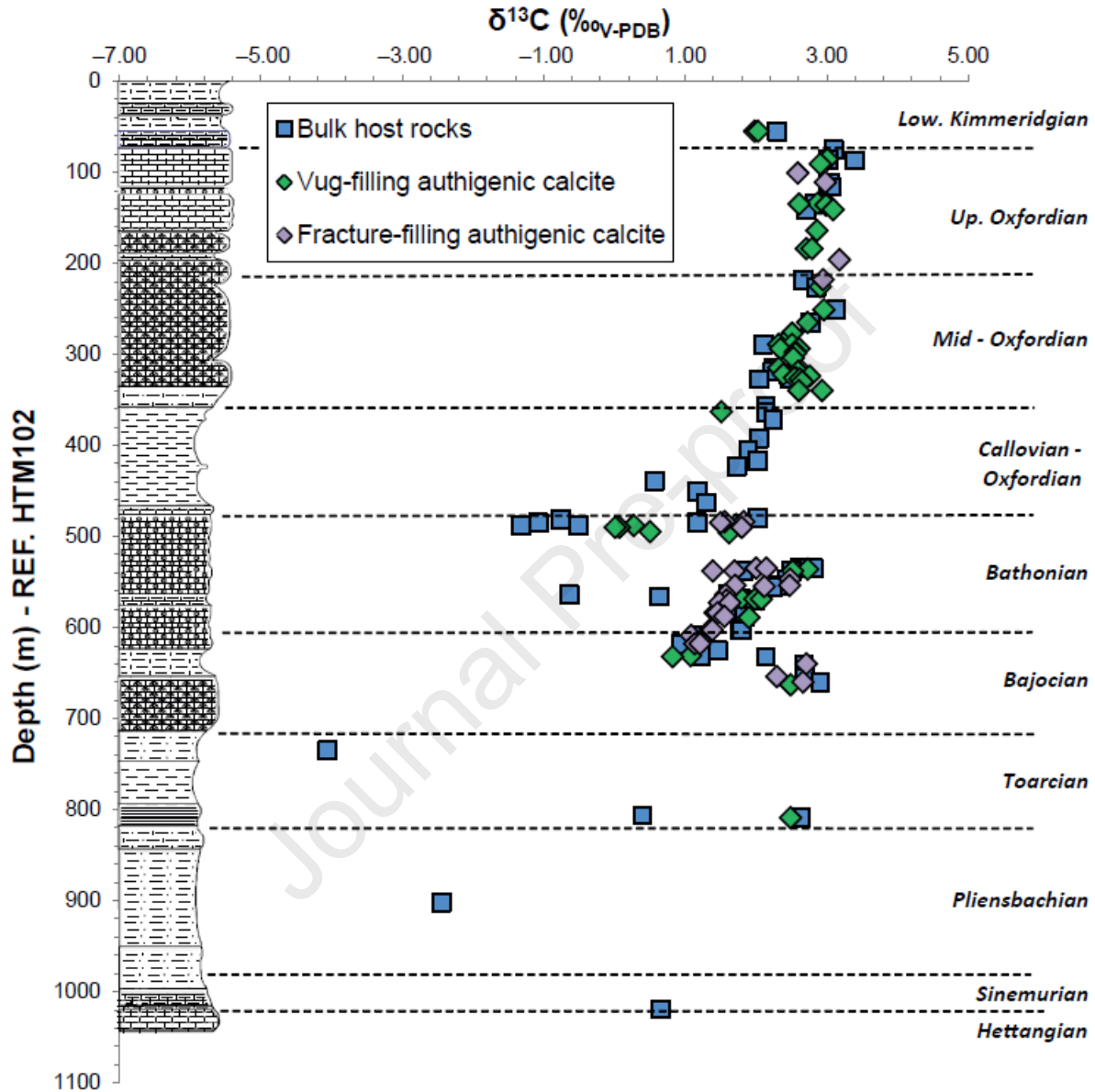
$\delta^{18}\text{O}$  and  $\delta^{13}\text{C}$

252 The  $\delta^{18}\text{O}$  values of the bulk calcite content in core samples from the MJL and UJL range  
 253 between  $-7.5$  and  $-0.9$  ‰  $\text{V-PDB}$  (Table 2). Oolitic or reefal limestones, where authigenic calcite  
 254 now fills the initial primary porosity, show the lowest values. Authigenic calcite extracted from  
 255 vugs and fractures exhibit  $\delta^{18}\text{O}$  values between  $-9.5$  and  $-6.2$  ‰  $\text{V-PDB}$  (Table 3), without  
 256 difference between vugs and fractures. All O and C stable isotope data from core samples are  
 257 plotted as a function of depth in Figure 6 and 7, respectively.





259 Figure 6. Vertical distribution of calcite  $\delta^{18}\text{O}$  (‰ V-PDB) values in authigenic infillings (vugs and  
 260 fractures) and bulk calcite in host limestones or marls. The depth scale of the well HTM102 is  
 261 used as a reference.



262  
 263 Figure 7. Vertical distribution of calcite  $\delta^{13}\text{C}$  (‰ V-PDB) values in authigenic infillings (vugs and  
 264 fractures) and bulk calcite in host limestones or marls. The depth scale of the well HTM102 is  
 265 used as a reference.

266 The  $\delta^{13}\text{C}$  values of bulk calcite in core samples from host rocks range from -18.3 to 2.9 ‰ V-PDB  
 267 (Table 2). Negative values of  $\delta^{13}\text{C}$  are found exclusively in the Bathonian limestones and the  
 268 underlying formations (the lowest value of -18.3 ‰ V-PDB was measured in the Pliensbachian  
 269 marls). The carbon isotope composition of authigenic calcite is usually very close to the bulk

value of the host rock, with a deviation typically less than 1 ‰<sub>V-PDB</sub> and no distinction between vugs or fractures infilling calcite.

The isotopic composition of bulk host rocks of outcrop samples was analyzed on two samples, giving  $\delta^{18}\text{O}$  of  $-6.1$  and  $-3.5$  ‰<sub>V-PDB</sub> and  $\delta^{13}\text{C}$  of  $1.7$  and  $2.8$  ‰<sub>V-PDB</sub> (Table 4).  $\delta^{18}\text{O}$  values of authigenic calcite range from  $-9.9$  to  $-8.5$  ‰<sub>V-PDB</sub>, while  $\delta^{13}\text{C}$  values range from  $1.1$  to  $2.7$  ‰<sub>V-PDB</sub> (Table 5).

Borehole	Depth (HTM102) m	Stratigraphic position	Lithology	$\delta^{18}\text{O}$	$\delta^{13}\text{C}$	$^{87}\text{Sr}/^{86}\text{Sr}$
EST433	319	Middle Oxfordian	Argillaceous reef limestone	-1.5	+2.2	
PAX	363	Lower Oxfordian	Marl	-0.9	+2.1	
EST433	481	Bathonian	Oolitic limestone	-7.5	-0.8	
EST433	485	Bathonian	Oolitic limestone	-5.0	-1.1	
id.	488	Bathonian	Oolitic limestone	-4.6	-1.3	
id.	488	Bathonian	Oolitic limestone	-5.2	-0.5	0.707168
EST433	564	Bathonian	Oolitic limestone	-4.7	-0.6	
id.	566	Bathonian	Oolitic limestone	-5.6	+0.6	0.707242
id.	568	Bathonian	Oolitic limestone	-4.4	+1.6	0.707162
id.	568	Bathonian	Oolitic limestone	-4.7	+1.8	
EST433	625	Bajocian	Oncolytic limestone	-4.1	+1.5	
EST433	632	Bajocian	Micritic limestone	-4.1	+2.1	
EST433	654	Bajocian	Reef limestone	-2.8	+2.7	0.707209
id.	660	Bajocian	Reef limestone	-2.7	+2.9	0.707307
id.	735	Middle Toarcian	Marl	-3.3	-4.1	0.707858
id.	807	Lower Toarcian	Marl	-5.2	+0.4	0.707344
id.	809	Pliensbachian	Marl	-3.1	+2.6	0.707213
id.	899	Pliensbachian	Marl	-4.4	-18.3	0.707723
id.	902	Pliensbachian	Marl	-4.1	-2.4	0.708086
id.	1019	Hettangian	Marl	-2.0	+0.6	0.707859

Table 2. O, C, and Sr isotope compositions of bulk host rocks from core samples.

Borehole	Depth (HTM102) m	Stratigraphic position	Sample type	Host lithology	$\delta^{18}\text{O}$	$\delta^{13}\text{C}$	$^{87}\text{Sr}/^{86}\text{Sr}$
PPA	134	Upper Oxfordian	Vug	Reef limestone	-8.7	+2.9	
id.	134	Upper Oxfordian	Vug	Reef limestone	-8.3	+3.0	
id.	134	Upper Oxfordian	Vug	Reef limestone	-8.3	+2.9	
PPA	184	Upper Oxfordian	Vug	Oolitic limestone	-9.1	+2.7	
id.	184	Upper Oxfordian	Vug	Oolitic limestone	-8.7	+2.8	
EST205	294	Middle Oxfordian	Vug	Reef limestone	-8.6	+2.3	0.707166
EST433	319	Middle Oxfordian	Vug	Argillaceous reef limestone	-9.4	+2.6	0.707305
EST205	322	Middle Oxfordian	Vug	Argillaceous reef limestone	-9.5	+2.4	0.707350
EST205	326	Middle Oxfordian	Vug	Argillaceous reef limestone	-9.1	+2.5	0.707310
EST205	330	Middle Oxfordian	Vug	Argillaceous reef limestone	-9.2	+2.7	0.707353
PPA	340	Middle Oxfordian	Vug	Argillaceous reef limestone	-9.4	+2.6	
PAX	340	Middle Oxfordian	Vug	Argillaceous reef limestone	-8.8	+2.9	
id.	363	Lower Oxfordian	Vug	Marl	-9.5	+1.5	
EST433	488	Bathonian	Moldic	Oolitic limestone	-8.5	+0.3	
EST433	490	Bathonian	Vug	Oolitic limestone	-9.5	+0.1	
id.	490	Bathonian	Vug	Oolitic limestone	-9.4	0.0	
id.	495	Bathonian	Vug	Oolitic limestone	-8.9	+0.5	0.707294
EST433	568	Bathonian	Vug	Oolitic limestone	-6.8	+1.8	0.707152
id.	569	Bathonian	Vug	Oolitic limestone	-6.6	+2.0	0.707249
id.	569	Bathonian	Vug	Oolitic limestone	-6.3	+2.1	0.707380
EST433	632	Bajocian	Moldic	Argillaceous limestone	-6.2	+0.8	
EST433	654	Bajocian	Micro-fracture	Argillaceous limestone	-6.6	+2.3	0.707311
id.	660	Bajocian	Micro-fracture	Argillaceous reef limestone	-6.6	+2.7	0.707244
id.	660	Bajocian	Micro-fracture	Argillaceous reef limestone			0.707365
EST433	809	Pliensbachian	Vug	Argillaceous limestone	-7.1	+2.5	0.707511

Table 3. O, C, and Sr isotope compositions of authigenic calcite from core samples.

Locality	Sample name	Stratigraphic position	$\delta^{18}\text{O}$	$\delta^{13}\text{C}$	$^{87}\text{Sr}/^{86}\text{Sr}$
Augeville	AB7-kim-E	Lower Kimmeridgian	-3.5	+1.7	0.707157
	AB7-E	Upper Oxfordian	-6.2	+2.8	0.707114

Table 4. O, C, and Sr isotope compositions of limestone from outcrop samples.

Locality	Sample Name	Stratigraphic position	Sample type	$\delta^{18}\text{O}$	$\delta^{13}\text{C}$	$^{87}\text{Sr}/^{86}\text{Sr}$
Augeville	AB7-GC-C	Upper Oxfordian	Fracture	-9.4	+2.0	0.707454
	AB7-GF-C	Upper Oxfordian	Fracture	-10.0	+1.6	0.707309
	AB7-CO-C	Upper Oxfordian	Breccia	-9.0	+2.0	0.707400
	AB7-PU-C	Upper Oxfordian	Breccia	-8.7	+2.5	0.707666
	AB7-N	Lower Kimmeridgian	Fracture	-8.4	+2.2	0.707508

Table 5. O, C, and Sr isotope compositions of authigenic calcite from outcrop samples.

## Discussion

Fluid flows and cementation processes

The conceptual diagenetic model proposed by Carpentier et al. (2014) highlights the role of propagating horizontal stress field in the opening of micro-fissures, which contributed to fluid flows and calcite precipitation. To better constrain the nature of paleo-fluids, Blaise et al. (2015) measured the  $\delta D$  value of aqueous fluid inclusions trapped in authigenic calcite crystals. This method confirmed the meteoric origin of fluids that precipitated calcite both in the UJL vugs and in the breccias and fractures along the Gondrecourt Graben ("AB7" site, Augeville locality, Figure 1). A second approach was used by Pagel et al. (2018), who measured the  $\Delta_{47}$  clumped isotope composition of calcite filling breccias and fractures along the Gondrecourt Graben (Figure 1), and confirmed the meteoric nature of parent waters with crystallization temperatures between  $41$  to  $46 \pm 3$  °C. Using the  $\delta D$  values from Blaise et al. (2015), Pagel et al. (2018) concluded that the isotopic composition of parent waters was shifted towards the right of the Global Meteoric Water Line (GMWL) in a  $\delta D$  vs  $\delta^{18}O$  diagram, hence revealing  $^{18}O$  exchange with host carbonates. Recently, Brigaud et al. (2020) measured the  $\Delta_{47}$  clumped isotope composition of vug-filling calcite in the MJL in wells EST433, EST210, EST205, and HTM102 (Figure 1). They documented much higher crystallization temperatures than previously estimated, up to  $110$  °C, and thus positive  $\delta^{18}O_{water}$ , which is interpreted to reflect flow of hydrothermal fluids along major, deeply-rooted faults in this part of the Basin.

The successive opening of fracture networks in the Jurassic limestones has played a crucial role in past fluid flows and calcite cementation (André et al., 2010). A key question is whether a change in the physical-chemical environment (e.g., pH, temperature) or the dissolution-recrystallization of host carbonate rocks triggered calcite saturation. The  $\delta^{13}C$  values of calcite cement from both vugs and fractures are very close to the  $\delta^{13}C$  values of the bulk calcite from the host limestones (Figure 7). A carbon of local origin was thus directly transferred from the host rock to the authigenic cement through calcite dissolution followed by subsequent calcite crystallization.

In the UJL, authigenic calcite in vugs and fractures shows similar oxygen isotope composition (Figure 6). These calcites crystallized during the Late Cretaceous to the Cenozoic period (Cal3 and Cal4 of Carpentier et al., 2014). At that time, the eastern part of the Paris Basin was already inverted, allowing the incursion of meteoric waters. The consistently high  $\delta^{18}O$  values reflects a meteoric origin at relatively low temperature (Blaise et al., 2015). It shows that the Upper Jurassic limestone acted as an opened hydrologic system, allowing large scale fluid-flows under high water-rock ratios.

By contrast, the highly variable  $\delta^{18}O$  values of authigenic calcite in the MJL (Figure 6) indicate that calcite cement crystallized either from different fluids or at different temperatures or both (Brigaud et al., 2009a, 2020, Carpentier et al., 2014). Figure 6 shows that a large portion of calcite in fractures displays the lowest  $\delta^{18}O$  values. This isotopic shift between fracture-filling calcite and host rocks could result from fast flows of allochthonous fluids and rapid crystallization under high water-rock ratios. We will use strontium isotope composition in the following section to test this hypothesis.

Constraints on strontium isotope ratios

To properly interpret Sr isotope data, one must consider the contribution of Sr from the desorption or partial dissolution of detrital materials due to nitric acid leaching (Cao et al., 2020). Petrographic observations show that calcite cements are free of detrital inclusions (Figure 4). ICP-OES analysis of four samples show K<sub>2</sub>O values below 0.04 % (Supplementary data). Host limestones may contain detrital clays, including mixed-layer illite/smectite (Carpentier, 2005). Bulk dissolution ICP-MS analyses by André (2003) reveal an Al<sub>2</sub>O<sub>3</sub> content lower than 0.3 % in the Upper Jurassic limestones. Our ICP-OES data on four bulk limestone samples give a K<sub>2</sub>O content of about 0.4 % for a single sample, while the three other samples display K<sub>2</sub>O < 0.1 %. Thus, detrital components are present in minute amounts in limestones. The desorption or partial dissolution of clay minerals during leaching in nitric acid would lead in higher <sup>87</sup>Sr/<sup>86</sup>Sr ratios in bulk limestones than the contemporaneous seawater, which is indeed observed here (Figure 5). However, the fact that inclusion-free calcite cements are enriched in radiogenic Sr compared to the bulk host limestones demonstrates that contamination from detrital clays is not significant, and that <sup>87</sup>Sr/<sup>86</sup>Sr ratios in both calcite cements and host limestones are largely dominated by the Sr recovered from calcite dissolution.

Marls and shales from Callovian-Oxfordian and Lower Jurassic units were also included in this study to determine the Sr isotope composition of their bulk calcite content. The obtained <sup>87</sup>Sr/<sup>86</sup>Sr ratios are on average higher than in bulk limestones, suggesting that a portion of the total Sr recovered from acid leaching comes from the desorption or partial dissolution of detrital minerals. Focusing on the Callovian-Oxfordian marls, the mean <sup>87</sup>Sr/<sup>86</sup>Sr value obtained from 8 samples after reaction with nitric acid is 0.707310 (Maes, 2002), much lower than the mean value of 0.717177 obtained by Lerouge et al. (2010) from the dissolution of the entire detrital fraction. Using a sequential extracting procedure, these authors measured the Sr isotope composition of the exchangeable Sr adsorbed on clay minerals (mean value of 0.7074365) and the Sr composition of calcite crystals (mean value of 0.707068) in Callovian-Oxfordian claystones. Based on this comparison, the Sr fraction recovered and analyzed in this study corresponds to the dissolution of calcite and the partial desorption of Sr in clays. Dissolution of mixed layer smectite/illite and K-feldspar is ruled out, as it would have generated much higher <sup>87</sup>Sr/<sup>86</sup>Sr values in marls and claystones. In the Upper and Middle Jurassic limestone units, the contribution of Sr desorption in clay minerals is negligible. As strontium isotopes do not fractionate during mineral precipitation, the higher <sup>87</sup>Sr/<sup>86</sup>Sr values recorded in calcite cements compared with host limestones (Figure 5) can thus be directly attributed to enrichment in <sup>87</sup>Sr in the diagenetic waters. Such enrichment in radiogenic Sr may result from several processes:

(1) Incursion of meteoric waters that interacted with siliciclastic or evaporitic sedimentary rocks (Brenot et al., 2008), crystalline basements (Prosser et al., 1993; Eikenberg et al., 2001), or soils (Pourcelot et al., 2008);

(2) Waters derived from deeper Triassic aquifers or basement fluids (Muñoz-López et al., 2020) injected into the shallower Jurassic carbonate aquifers, as evidenced in the central Paris Basin (Fontes and Matray, 1993a, 1993b; Worden and Matray, 1995);

(3) Local enrichment due to Sr desorption from the clay fraction distributed in limestones, or pore water expulsion during mechanical compaction or stylolitization;

(4) Sr diffusion from clay-rich rocks (Callovian-Oxfordian and Liassic claystones and marls).

#### *Sr isotope composition of calcite cements in the Upper Jurassic limestones*

Sr diffusion from clay-rich units is an unlikely source of  $^{87}\text{Sr}$  enrichment, as it would generate much more homogenous  $^{87}\text{Sr}/^{86}\text{Sr}$  ratios than what is observed in the limestone groundwaters. Furthermore, no Sr diffusion profile is observed from the Callovian-Oxfordian claystones to the Upper and Middle Jurassic limestone aquifers (Lerouge et al., 2010). The interaction of continental waters with outcropping crystalline and sedimentary formations during their surface flow and infiltration constitutes another source of radiogenic Sr. Present-day rivers draining the East of the studied area have more radiogenic strontium ( $^{87}\text{Sr}/^{86}\text{Sr} > 0.708$ ; e.g., Brenot et al., 2008) than the one of groundwaters in the Upper and Middle Jurassic limestones ( $^{87}\text{Sr}/^{86}\text{Sr}$  between 0.707080 and 0.707152, and between 0.707261 and 0.707375, respectively; Rebeix et al., 2011). The Sr isotope composition of groundwaters is therefore controlled at first order by the water - limestone interaction. The hydrological processes can be assumed to be similar in the past, at least regarding the Cenozoic period, as the geometry of sedimentary strata were comparable to the present-day one. Thus, past groundwaters were similarly buffered by carbonates and should have had comparable  $^{87}\text{Sr}/^{86}\text{Sr}$  to the present ones.

Therefore, the preferred source of  $^{87}\text{Sr}$  in the Upper Jurassic limestones is the allochthonous fluids coming from deeper reservoirs, channelled along major regional faults and penetrating the limestones through the fracture networks. Such “cross-formational flow” was demonstrated in the central and eastern part of the Paris Basin from the chemistry of present-day groundwaters and the Sr, C, O and clumped isotope composition of calcite cements (Worden and Matray, 1995, Mangenot et al., 2018, Brigaud et al., 2020). It is also recorded in fluid inclusions trapped in authigenic carbonates and quartz (Bril et al., 1994; Demars and Pagel, 1994). To test this hypothesis, we investigated the isotopic composition of calcite in hydraulic breccias and fractures affecting the UJL along the Gondrecourt graben at the Augeville locality situated about 10 km south of the URL (“AB7” samples, Figure 1). Calcite filling hydraulic breccias were dated by *in situ* U-Pb geochronology at  $43 \pm 1$  Ma, while calcite in fractures yields an age of  $34.9 \pm 1.2$  Ma (Pagel et al., 2018). The younger generation matches the ID-TIMS U-Pb age of  $33.5 \pm 2.8$  Ma obtained on vug-filling calcite in the Upper Jurassic limestone in wells EST205 and HTM102 (Pisapia et al., 2017). Calcite infillings along the Gondrecourt graben and in the Upper Jurassic limestone vugs also have similar fluid inclusions  $\delta\text{D}$  composition (Blaise et al., 2015). Therefore, they share probably a common origin, *i.e.*, they were precipitated from the same fluids simultaneously, during the Eocene-Oligocene transpressional to extensional regime period. The  $\delta^{18}\text{O}$  and  $^{87}\text{Sr}/^{86}\text{Sr}$  data, as illustrated in Figure 8, yield the same conclusion. Authigenic calcite filling vugs in borehole samples and calcite filling breccias and fractures along the Gondrecourt graben show identical  $\delta^{18}\text{O}$  and variable  $^{87}\text{Sr}/^{86}\text{Sr}$ . This variability in  $^{87}\text{Sr}/^{86}\text{Sr}$  ratios may result from the mixing of two different water sources, an autochthonous low-radiogenic Upper Jurassic limestone porewater, and a more radiogenic source, likely the underlying Triassic waters. Triassic rocks are indeed mainly composed of evaporite and siliciclastic layers having bulk  $^{87}\text{Sr}/^{86}\text{Sr} > 0.708$  (Table 1). Present-day groundwaters in the Lower Triassic sandstones have



$^{87}\text{Sr}/^{86}\text{Sr} = 0.712856$  and a Sr concentration of  $163 \text{ mg.L}^{-1}$ , around forty times higher than the mean Sr concentration of dissolved Sr in the present-day groundwaters of the UJL (Rebeix et al., 2011). Therefore, the variable Sr isotope composition recorded in calcite may result from variable mixing proportions between the two fluids. The Triassic fluids were highly diluted in the Upper Jurassic limestone porewaters. Consistently, Cl concentration is low in calcite fluid inclusions from the Gondrecourt graben and Upper Jurassic boreholes (less than  $150 \text{ mmol l}^{-1}$ , Blaise et al., 2015).

Besides variable mixing proportions, a second parameter that can explain the highly variable  $^{87}\text{Sr}/^{86}\text{Sr}$  recorded in calcite crystals is the fluid-rock ratios. As calcite crystallized, the available pore space decreased, together with the fluid-rock ratio. The allochthonous fluid progressively equilibrated through the dissolution-recrystallisation of the host limestone and mixed with the autochthonous and isotopically-equilibrated groundwater. During the Cenozoic period, the Gondrecourt fault, located at the vicinity of HTM102, EST210, EST205 or EST433 borehole (2, 4, 5 and 11 km, respectively) probably favoured the ascension of the deep, allochthonous fluids. A synthetic conceptual model is proposed in Figure 9.

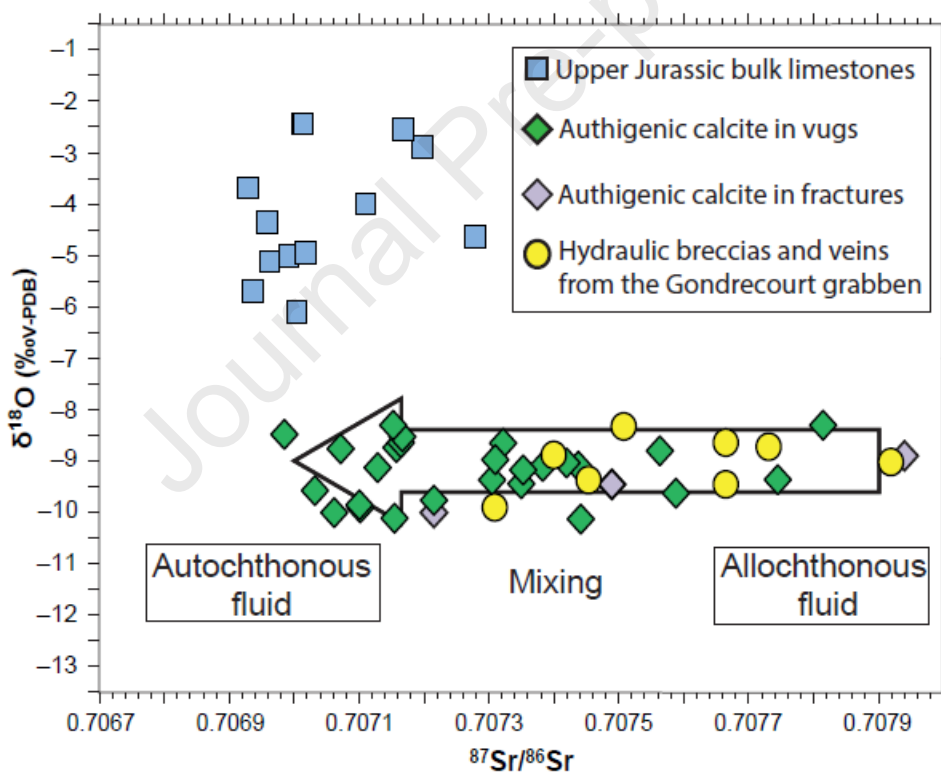


Figure 8.  $^{87}\text{Sr}/^{86}\text{Sr}$  vs  $\delta^{18}\text{O}$  (‰V-PDB) of authigenic calcite and bulk calcite content in host rocks in the UJL.

433

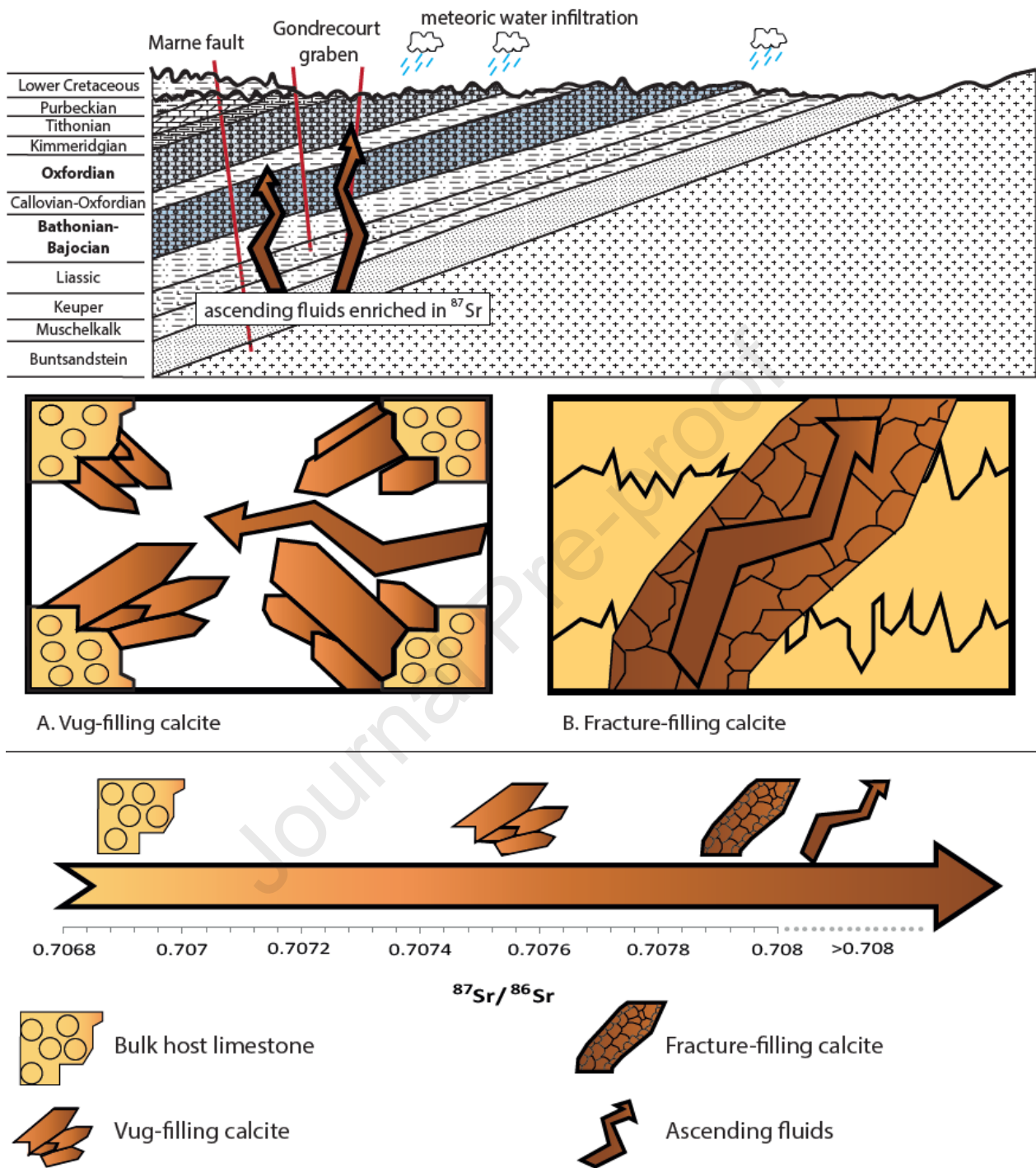


Figure 9. A conceptual model for the crystallization of calcite cements in the UJL. The geometry of the basin corresponds to the Eocene-Oligocene main cementation event.

437

*Sr isotope composition of calcite cements in the Middle Jurassic limestones*

As recently evidenced by Brigaud et al. (2020), early calcite-mineralizing fluids (Cal1 and Cal2, Table 1) in the MJL were in thermal disequilibrium with the host rocks. The unexpectedly high temperatures detected by  $\Delta_{47}$  clumped isotopes thermometry also led to different estimates of the  $\delta^{18}\text{O}$  values of the parent waters (Brigaud et al., 2020), thus giving a completely different view of the cementation history in the MJL. In the light of these recent data, the injection of warm waters from deeper Triassic aquifers, appears likely. Because crystallization temperatures can be highly variable (from 30 to  $109 \pm 6$  °C, according to Brigaud et al., 2020), the  $\delta^{18}\text{O}$  values of authigenic calcite in the MJL cannot readily be interpreted. For instance, ranges in the  $\delta^{18}\text{O}$  values of calcite could be interpreted as precipitated from fluids having distinct origins or a single fluid undergoing progressive cooling.

In Figure 10, where the  $\delta^{18}\text{O}$  value is plotted as a function of the  $^{87}\text{Sr}/^{86}\text{Sr}$  ratio,  $^{87}\text{Sr}$  enrichment is much more pronounced in calcite filling fractures than in calcite filling vugs. As in Figure 8, data distribution in Figure 10 may be interpreted as a mixing trend between two fluid end-members of distinct composition. The first generations of authigenic calcite (Cal1 and Cal2, Table 1) may have crystallized from the mixing between an  $^{87}\text{Sr}$ -rich allochthonous deep fluid and the autochthonous connate waters. This hypothesis is supported by the high salinity of fluid inclusions from MJL calcite (Blaise et al., 2015). For Cal3 and Cal4 (Table1), a scenario similar to the UJL is also likely, with new injections of deep fluids mixing with local freshwaters (Figure 9). Indeed, calcites Cal3 and Cal4 have comparable  $^{87}\text{Sr}/^{86}\text{Sr}$  in the UJL and MJL. Actually, carbonate diagenesis mediated by freshwaters or basinal brines is known to produce such an isotopic shift towards lower  $\delta^{18}\text{O}$  and higher  $^{87}\text{Sr}/^{86}\text{Sr}$  (Moldovanyi et al., 1990; Barker et al., 2009; Faÿ-Gomord et al., 2018; Zhu et al., 2019).

Similar to the UJL, we propose that the fluid-rock ratio is the second-order parameter controlling the  $^{87}\text{Sr}/^{86}\text{Sr}$  composition of calcite in the MJL. Fast advective flow may have favoured the circulation of warm water enriched in radiogenic Sr. During the Late Jurassic, ascendant fluid flows could have been driven by the presence of fault conduits such as Vittel or Marne faults, located about 20 km from the study area. Fluids could have impregnated the Middle Jurassic carbonate aquifers from these permeable faults. Gradual cooling together with chemical equilibration with host limestones and dilution by autochthonous freshwater may then have equilibrated the isotopic composition of calcite-mineralizing waters.

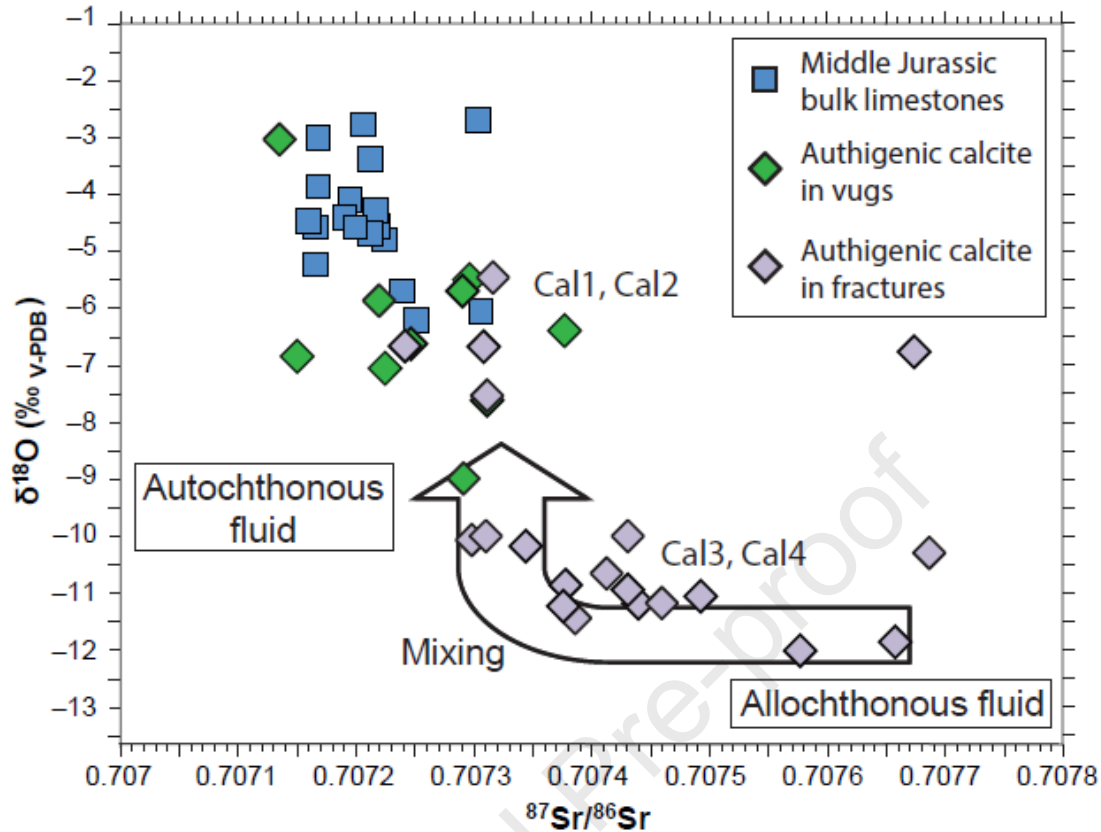


Figure 10.  $^{87}\text{Sr}/^{86}\text{Sr}$  vs  $\delta^{18}\text{O}$  (‰V-PDB) of authigenic calcite and bulk calcite content in host rocks in the MJL.

#### Evolution of the hydrologic system towards present-day conditions

Paleo-water flows that have cemented the Jurassic limestones were in thermal (Pagel et al., 2018; Brigaud et al., 2020) and isotopic disequilibrium (this study) with the host rocks. The crystallization of authigenic calcite cement has thus strongly modified the bulk isotopic composition of the limestones. As illustrated in Figure 11, the  $^{87}\text{Sr}/^{86}\text{Sr}$  ratio of calcite in the Jurassic limestones is higher than the contemporaneous seawater  $^{87}\text{Sr}/^{86}\text{Sr}$  ratio (Jones et al., 1994a, 1994b). This increase is mainly due to the contribution of calcite cements enriched in  $^{87}\text{Sr}$ . In both limestone aquifers, the present-day  $^{87}\text{Sr}/^{86}\text{Sr}$  ratio of present-day groundwaters is relatively homogenous (Rebeix et al., 2011). Such homogeneity is explained by long-term isotopic equilibration. The residence times of present-day water are estimated at about 10 ka, in the UJL and several hundred thousand years in the MJL (Lavastre et al., 2010).

By contrast, the  $^{87}\text{Sr}/^{86}\text{Sr}$  ratios of paleo-fluids recorded in authigenic calcite (Figure 11) are much more dispersed than the ratios of present-day groundwaters. A change in hydrological regimes may explain such a difference through time. As discussed in previous sections, the primary vector of calcite-mineralizing waters was the fracture network that opened during major

geodynamical events that affected the eastern Paris Basin (Carpentier et al., 2014). Fast fluid flows under high water-rock ratios and subsequent fracture sealing prevented isotopic equilibration between the fluid and its host limestone (Cole, 1994). The water fluxes were likely supplied along the major regional faults (Gondrecourt, Marne, and Vittel faults, Figure 1). The microcracks were successively sealed as they formed. When compressive stresses decreased, the penetration of allochthonous waters stopped due to microfracture network closing. An obvious consequence of calcite cementation is the progressive reduction of pore size. At present, groundwaters in both limestone units flow through microporous sub-zones (Brigaud et al., 2009b; Carpentier et al., 2014), favouring isotopic equilibration by dissolution-crystallisation and small-scale diffusion of Sr. The isotopic re-equilibration of present-day groundwaters occurs through a fluid - bulk calcite interaction, the bulk calcite including a variable proportion of authigenic cements with high  $^{87}\text{Sr}/^{86}\text{Sr}$  ratios.

At present, chemical transfer of gas and solutes through the Callovian-Oxfordian claystones are interpreted as controlled mainly by diffusion processes (Lavastre et al., 2005; Rebeix et al., 2011, Battani et al., 2011; Fourré et al., 2011; Bencenouci et al., 2011; Mazurek et al., 2011). The original connate water is now replaced by meteoric water (Gianessini, 2006). As illustrated in Figure 11, the  $^{87}\text{Sr}/^{86}\text{Sr}$  values of the present-day Callovian-Oxfordian porewater (Vinsot et al., 2008) are much higher than the values recorded in the carbonate fraction (Lerouge et al., 2010). Indeed, this carbonate fraction is mainly composed of primary micrite, and early diagenetic cements precipitated under equilibrium with the original Callovian-Oxfordian seawater.  $^{87}\text{Sr}/^{86}\text{Sr}$  in the authigenic celestite is primarily in the range of the pristine Callovian-Oxfordian seawater, except for a single crystal interpreted as late diagenetic in origin (Figure 11, Lerouge et al., 2010). The source of  $^{87}\text{Sr}$ -richness in the present-day Callovian-Oxfordian porewater is still debated. Lerouge et al. (2010) suggested that it is controlled by the exchangeable strontium from illite and illite/smectite mixed-layer surfaces. The dissolution of detrital K-micas and feldspar grains may also have contributed to the release of  $^{87}\text{Sr}$  in porewater (Lerouge et al., 2010). Another hypothesis is Sr diffusion from underlying limestone aquifers. Although not favoured, this hypothesis was mentioned by Lerouge et al. (2010), taking into account the Sr isotope composition of groundwaters in the MJL measured by Fontes and Matray (1993a, 1993b). When considering the lower  $^{87}\text{Sr}/^{86}\text{Sr}$  ratios of groundwaters measured in the studied area by Rebeix et al. (2011) plotted in Figure 11, this hypothesis appears even less likely. However, such diffusion of Sr with high  $^{87}\text{Sr}/^{86}\text{Sr}$  ratios could have well occurred in the past. Indeed, the Sr isotope composition of the paleo-fluids recorded in the authigenic calcite matches Callovian-Oxfordian porewater composition. The fact that Sr may have diffused from the overlying and underlying limestone aquifers through the Callovian-Oxfordian claystones in the past constitutes another hypothesis to explain the  $^{87}\text{Sr}$  enrichment measured in the exchangeable fraction and the porewater.

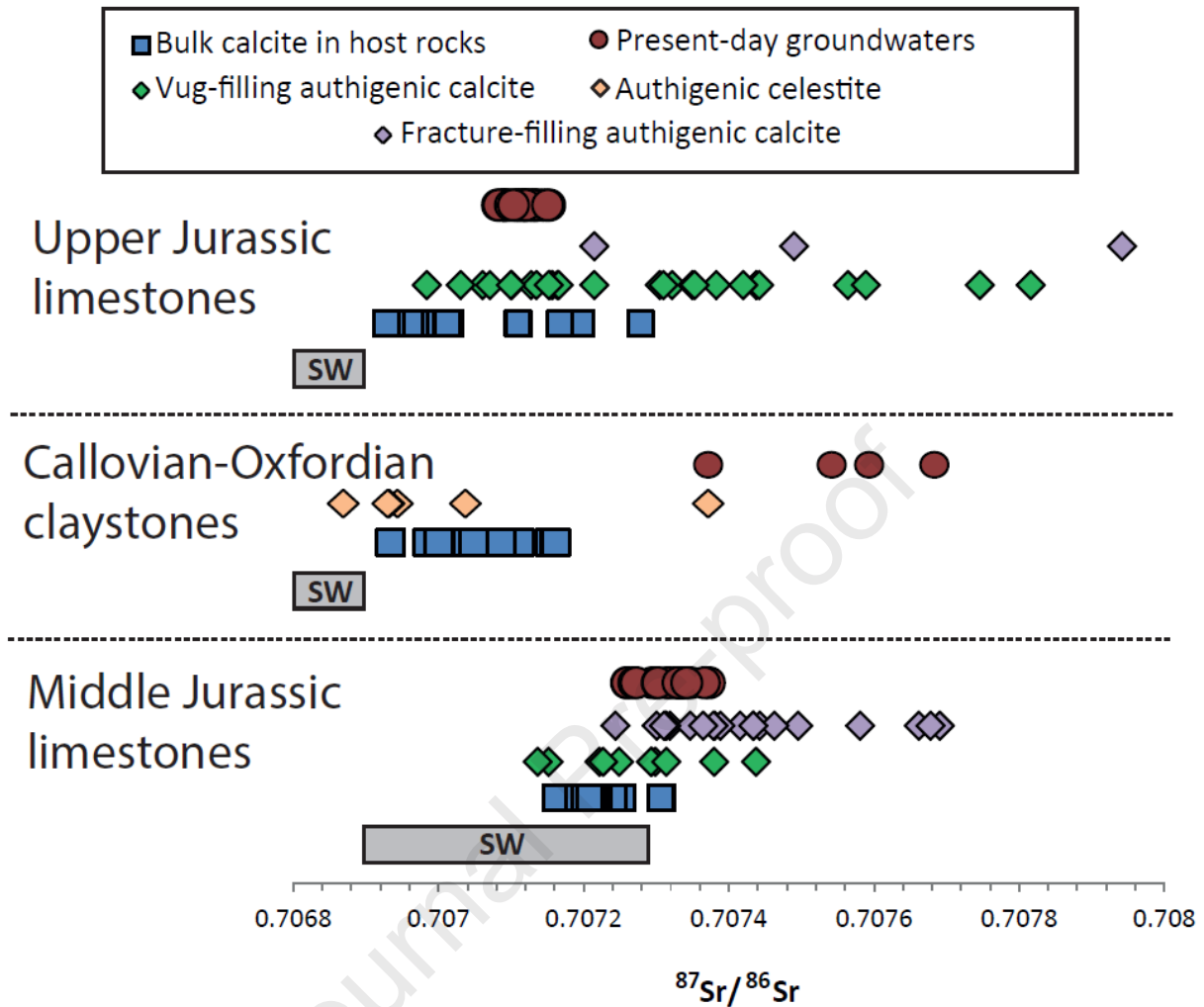


Figure 11.  $^{87}\text{Sr}/^{86}\text{Sr}$  values of (1) authigenic calcite in both vugs and fractures, (2) the bulk calcite content of host rocks in the Middle and Upper Jurassic limestones (this study) and the Callovian-Oxfordian claystones (Lerouge et al., 2010), (3) Present-day groundwaters in the Middle and Upper Jurassic limestones (Rebeix et al., 2011), (4) Present-day porewater in the Callovian-Oxfordian claystones (Vinsot et al., 2008), (5) Authigenic celestite in the Callovian-Oxfordian claystones (Lerouge et al., 2010). SW: average seawater values (Jones et al., 1994a, 1994b).

## Conclusions

Conclusions derived from this study include:

- The shift to  $^{87}\text{Sr}$ -enrichment in calcite cement is attributed to an allochthonous fluid contribution from deeper levels through the major regional faults. The more pervasive percolation in Jurassic reservoirs was facilitated by a fracture network that increased the limestone permeability.



- Paleo-waters were enriched in  $^{87}\text{Sr}$  compared to the host limestones and present-day groundwaters. In the Middle Jurassic limestones, this enrichment is higher in fractures compared to vugs.
- The strontium isotope shift between the authigenic calcite and the host limestones depended on the dilution rate of radiogenic allochthonous fluids by the limestone porewaters.
- These paleo-water flows may also have contributed to the diffusion of strontium through the Callovian-Oxfordian claystones.
- At present, the fracture network is sealed, and groundwaters flowing through the microporous layers of the Middle and Upper Jurassic limestones is at Sr isotope equilibrium with the bulk host limestone.

## Acknowledgements

This study is a part of Andra and TAPSS 2000 research program “Present and past transfers in a sedimentary aquifer–aquitard system: a 2000 m deep drill-hole in the Mesozoic of the Paris Basin”. It was funded by GNR FORPRO and a PhD grant obtained by the first author from Andra (French Agency for radioactive waste management). We are grateful to Executive Editor Dr. Zimeng Wang and associate editor Dr. Dmitrii Kulik. The manuscript greatly benefited from the careful review of an anonymous reviewer.

## References

- André, G., 2003. Caractérisation des déformations méso-cénozoïques et des circulations de fluides dans l'Est du Bassin de Paris. *Thèse de l'Université de Nancy*, 311 pp.
- André, G., Hibsach, C., Fourcade, S., Cathelineau, M., Buschaert, S., 2010. Chronology of fracture sealing under a meteoric fluid environment: Microtectonic and isotopic evidence of major Cainozoic events in the eastern Paris Basin (France). *Tectonophysics* 490, 214–228. <https://doi.org/10.1016/j.tecto.2010.05.016>
- Banner, J.L., 1995. Application of the trace element and isotope geochemistry of strontium to studies of carbonate diagenesis. *Sedimentology* 42, 805–824. <https://doi.org/10.1111/j.1365-3091.1995.tb00410.x>
- Barker, S.L.L., Bennett, V.C., Cox, S.F., Norman, M.D., Gagan, M.K., 2009. Sm-Nd, Sr, C and O isotope systematics in hydrothermal calcite–fluorite veins: Implications for fluid–rock reaction and geochronology. *Chemical Geology* 268, 58–66. <https://doi.org/10.1016/j.chemgeo.2009.07.009>
- Battani, A., Smith, T., Robinet, J.C., Brulhet, J., Lavielle, B., Coelho, D., 2011. Contribution of logging tools to understanding helium porewater data across the Mesozoic sequence of the East of the Paris Basin. *Geochimica et Cosmochimica Acta* 75, 7566–7584. <https://doi.org/10.1016/j.gca.2011.09.032>
- Beaudoin, N., Labeur, A., Lacombe, O., Koehn, D., Billi, A., Hoareau, G., Boyce, A., John, C.M., Marchegiano, M., Roberts, N.M., Millar, I.L., Claverie, F., Pecheyran, C., Callot, J.-P., 2020. Regional-scale paleofluid system across the Tuscan Nappe–Umbria–Marche Apennine Ridge (northern Apennines) as revealed by mesostructural and isotopic analyses of stylolite–vein networks. *Solid Earth*, 11, 1617–1641. <https://doi.org/10.5194/se-11-1617-2020>
- Blaise, T., Barbarand, J., Kars, M., Ploquin, F., Aubourg, C., Brigaud, B., Cathelineau, M., El Albani, A., Gautheron, C., Izart, A., Janots, D., Michels, R., Pagel, M., Pozzi, J.-P., Boiron, M.-C., Landrein, P., 2014. Reconstruction of low temperature (<100 °C) burial in

- sedimentary basins: A comparison of geothermometer in the intracontinental Paris Basin. *Marine and Petroleum Geology* 53, 71–87. <https://doi.org/10.1016/j.marpetgeo.2013.08.019>
- Blaise, T., Tarantola, A., Cathelineau, M., Boulvais, P., Techer, I., Rigaudier, T., Boiron, M.-C., Pierron, O., Landrein, P., 2015. Evolution of porewater composition through time in limestone aquifers: Salinity and D/H of fluid inclusion water in authigenic minerals (Jurassic of the eastern Paris Basin, France). *Chemical Geology* 417, 210–227. <https://doi.org/10.1016/j.chemgeo.2015.10.014>
- Blyth, A., Frape, S., Blomqvist, R., Nissinen, P., 2000. Assessing the past thermal and chemical history of fluids in crystalline rock by combining fluid inclusion and isotopic investigations of fracture calcite. *Applied Geochemistry* 15, 1417–1437. [https://doi.org/10.1016/S0883-2927\(00\)00007-X](https://doi.org/10.1016/S0883-2927(00)00007-X)
- Brand, U., Azmy, K., Tazawa, J., Sano, H., Buhl, D., 2010. Hydrothermal diagenesis of Paleozoic seamount carbonate components. *Chemical Geology* 278, 173–185. <https://doi.org/10.1016/j.chemgeo.2010.09.010>
- Brenot, A., Cloquet, C., Vigier, N., Carignan, J., France-Lanord, C., 2008. Magnesium isotope systematics of the lithologically varied Moselle river basin, France. *Geochimica et Cosmochimica Acta* 72, 5070–5089. <https://doi.org/10.1016/j.gca.2008.07.027>
- Brigaud, B., Bonifacie, M., Pagel, M., Blaise, T., Calmels, D., Haurine, F., Landrein, P., 2020. Past hot fluid flows in limestones detected by  $\Delta 47$ –(U–Pb) and not recorded by other geothermometers. *Geology* 48, 851 – 856. <https://doi.org/10.1130/G47358.1>
- Brigaud, B., Durllet, C., Deconinck, J.-F., Vincent, B., Pucéat, E., Thierry, J., Trouiller, A., 2009a. Facies and climate/environmental changes recorded on a carbonate ramp: A sedimentological and geochemical approach on Middle Jurassic carbonates (Paris Basin, France). *Sedimentary Geology* 222, 181–206. <https://doi.org/10.1016/j.sedgeo.2009.09.005>
- Brigaud, B., Durllet, C., Deconinck, J.-F., Vincent, B., Thierry, J., Trouiller, A., 2009b. The origin and timing of multiphase cementation in carbonates: Impact of regional scale geodynamic events on the Middle Jurassic Limestones diagenesis (Paris Basin, France). *Sedimentary Geology* 222, 161–180. <https://doi.org/10.1016/j.sedgeo.2009.09.002>
- Brigaud, B., Vincent, B., Carpentier, C., Robin, C., Guillocheau, F., Yven, B., Huret, E., 2014. Growth and demise of the Jurassic carbonate platform in the intracratonic Paris Basin (France): Interplay of climate change, eustasy and tectonics. *Marine and Petroleum Geology* 53, 3–29. <https://doi.org/10.1016/j.marpetgeo.2013.09.008>
- Bril, H., Velde, B., Meunier, A., Iqdari, A., 1994. Effects of the « Pays de Bray » fault on fluid paleocirculations in the Paris Basin Dogger Reservoir, France. *Geothermics* 23, 305–315. [https://doi.org/10.1016/0375-6505\(94\)90006-X](https://doi.org/10.1016/0375-6505(94)90006-X)
- Buschaert, S., Fourcade, S., Cathelineau, M., Deloule, E., Martineau, F., Ayt Ougougdal, M., Trouiller, A., 2004. Widespread cementation induced by inflow of continental water in the eastern part of the Paris basin: O and C isotopic study of carbonate cements. *Applied Geochemistry* 19, 1201–1215. <https://doi.org/10.1016/j.apgeochem.2003.01.001>
- Cao, C., Liu, X.-M., Bataille, C., Liu, C., 2020. What do Ce anomalies in marine carbonates really mean? A perspective from leaching experiments. *Chemical Geology* 532, <https://doi.org/10.1016/j.chemgeo.2019.119413>.
- Carpentier, C., Brigaud, B., Blaise, T., Vincent, B., Durllet, C., Boulvais, P., Pagel, M., Hibschi, C., Yven, B., Lach, P., Cathelineau, M., Boiron, M.-C., Landrein, P., Buschaert, S., 2014. Impact of basin burial and exhumation on Jurassic carbonates diagenesis on both sides of a thick clay barrier (Paris Basin, NE France). *Marine and Petroleum Geology* 53, 44–70. <https://doi.org/10.1016/j.marpetgeo.2014.01.011>
- Chen, Z., Hartmann, A., Wagener, T., Goldscheider, N., 2018. Dynamics of water fluxes and storages in an Alpine karst catchment under current and potential future climate

- conditions. *Hydrology and Earth System Sciences* 22, 3807–3823.  
<https://doi.org/10.5194/hess-22-3807-2018>
- Cole, D.R., 1994. Evidence for oxygen isotope disequilibrium in selected geothermal and hydrothermal ore deposit systems. *Chemical Geology* 111, 283–396.  
[https://doi.org/10.1016/0009-2541\(94\)90095-7](https://doi.org/10.1016/0009-2541(94)90095-7)
- Davis, D.W., Sutcliffe, C.N., Thibodeau, A.M., Spalding, J., Schneider, D., Cruden, A., Adams, J., Parmenter, A., Jensen, M., Zajacz, Z., 2020. Hydrochronology of a proposed deep geological repository for low- and intermediate-level nuclear waste in southern Ontario from U–Pb dating of secondary minerals: response to Silurian and Cretaceous events. *Canadian Journal of Earth Sciences* 57, 464–476. <https://doi.org/10.1139/cjes-2019-0004>
- de Haller, A., Tarantola, A., Mazurek, M., Spangenberg, J., 2011. Fluid flow through the sedimentary cover in northern Switzerland recorded by calcite–celestite veins (Oftringen borehole, Olten). *Swiss Journal of Geosciences* 104, 493–506.  
<https://doi.org/10.1007/s00015-011-0085-x>
- Debenham, N., Holford, S.P., King, R.C., 2020. The spatial distribution and geochemical variation of fault and fracture hosted calcite and gypsum cements in the eastern Bristol Channel Basin. *Marine and Petroleum Geology* 116, 104320.  
<https://doi.org/10.1016/j.marpetgeo.2020.104320>
- Demars, C., Pagel, M., 1994. Paleotemperatures and paleosalinities in the Keuper sandstones of the Paris Basin: fluid inclusions in authigenic minerals. *Compte Rendu de l'Académie des Sciences de Paris* 319, 427–434.
- Drake, H., Tullborg, E.-L., Hogmalm, K.J., Åström, M.E., 2012. Trace metal distribution and isotope variations in low-temperature calcite and groundwater in granitoid fractures down to 1km depth. *Geochimica et Cosmochimica Acta* 84, 217–238.  
<https://doi.org/10.1016/j.gca.2012.01.039>
- Drake, H., Kooijman, E., Kielman-Schmitt, M., 2020. Using  $^{87}\text{Sr}/^{86}\text{Sr}$  LA-MC-ICP-MS Transects within Modern and Ancient Calcite Crystals to Determine Fluid Flow Events in Deep Granite Fractures. *Geosciences* 10(9), 345.  
<https://doi.org/10.3390/geosciences10090345>
- Dublyansky, Y.V., Spötl, C., 2010. Evidence for a hypogene paleohydrogeological event at the prospective nuclear waste disposal site Yucca Mountain, Nevada, USA, revealed by the isotope composition of fluid-inclusion water. *Earth and Planetary Science Letters* 289, 583–594. <https://doi.org/10.1016/j.epsl.2009.11.061>
- Eikenberg, J., Tricca, A., Vezzu, G., Stille, P., Bajo, S., Ruethi, M., 2001.  $^{228}\text{Ra}/^{226}\text{Ra}/^{224}\text{Ra}$  and  $^{87}\text{Sr}/^{86}\text{Sr}$  isotope relationships for determining interactions between ground and river water in the upper Rhine valley. *Journal of Environmental Radioactivity* 54, 133–162. [https://doi.org/10.1016/S0265-931X\(00\)00171-5](https://doi.org/10.1016/S0265-931X(00)00171-5)
- Erhardt, A.M., Turchyn, A.V., Dickson, J.A.D., Sadekov, A.Y., Taylor, P.D., Wilson, M.A., Scott, P., Schrag, D.P., 2020. Chemical Composition of Carbonate Hardground Cements as Reconstructive Tools for Phanerozoic Pore Fluids. *Geochemistry, Geophysics, Geosystems* 21. <https://doi.org/10.1029/2019GC008448>
- Faÿ-Gomord, O., Allanic, C., Verbiest, M., Honlet, R., Champenois, F., Bonifacie, M., Chaduteau, C., Wouters, S., Muchez, P., Lasseur, E., Swennen, R., 2018. Understanding Fluid Flow during Tectonic Reactivation: An Example from the Flamborough Head Chalk Outcrop (UK). *Geofluids* 2018, 1–17.  
<https://doi.org/10.1155/2018/9352143>
- Ferry, S., Pellenard, P., Collin, P.-Y., Thierry, J., Marchand, D., Deconinck, J.-F., Robin, C., Carpentier, C., Durlet, C., Curial, A., 2007. Synthesis of recent stratigraphic data on Bathonian to Oxfordian deposits of the eastern Paris basin. *Mémoire de la Société*

- Géologique de France, n.S, n° 178, 37- 57.
- Fontes, J.C., Matray, J.M., 1993a. Geochemistry and origin of formation brines from the Paris basin, France. I. Brines associated with Triassic salts. *Chemical Geology* 109, 149–175. [https://doi.org/10.1016/0009-2541\(93\)90068-T](https://doi.org/10.1016/0009-2541(93)90068-T)
- Fontes, J.C., Matray, J.M., 1993b. Geochemistry and origin of formation brines from the Paris basin, France. II. Saline solutions associated with oil fields. *Chemical Geology* 109, 177–200. [https://doi.org/10.1016/0009-2541\(93\)90069-U](https://doi.org/10.1016/0009-2541(93)90069-U)
- Fourré, E., Jean-Baptiste, P., Dapoigny, A., Lavielle, B., Smith, T., Thomas, B., Vinsot, A., 2011. Dissolved helium distribution in the Oxfordian and Dogger deep aquifers of the Meuse/Haute-Marne area. *Physics and Chemistry of the Earth, Parts A/B/C* 36, 1511–1520. <https://doi.org/10.1016/j.pce.2011.10.006>
- Gély, J.-P., and Hanot, F., 2014. Coupe géologique du Bassin parisien et du Fossé rhénan: Bulletin d'Information des Géologues du Bassin de Paris, Mémoire hors-série no. 9, 1 planche.
- Giannesini, S., 2006. Géochimie isotopique couplée des eaux des formations argileuses et calcaires du site Andra de Meuse/Haute-Marne (PhD thesis), Paul Cezanne University, Aix-Marseille, France (291 pp.).
- Goldscheider, N., Chen, Z., Auler, A.S., Bakalowicz, M., Broda, S., Drew, D., Hartmann, J., Jiang, G., Moosdorf, N., Stevanovic, Z., Veni, G., 2020. Global distribution of carbonate rocks and karst water resources. *Hydrogeology Journal* 28, 1661–1677. <https://doi.org/10.1007/s10040-020-02139-5>
- Goodfellow, B.W., Viola, G., Bingen, B., Nuriel, P., Kylander-Clark, A.R.C., 2017. Palaeocene faulting in SE Sweden from U-Pb dating of slickenfibres calcite. *Terra Nova* 29, 321–328. <https://doi.org/10.1111/ter.12280>
- Guillocheau, F., Robin, C., Allemand, P., Bourquin, S., Brault, N., Dromart, G., Friedenberg, R., Garcia, J.-P., Gaulier, J.-M., Gaumet, F., Grosdoy, B., Hanot, F., Le Strat, P., Mettraux, M., Nalpas, T., Prijac, C., Rigollet, C., Serrano, O., Grandjean, G., 2000. Meso-Cenozoic geodynamic evolution of the Paris basin: 3D stratigraphic constraints. *Geodinamica Acta* 13, 189–246.
- Jones, C.E., Jenkyns, H.C., Hesselbo, S.P., 1994a. Strontium isotopes in early Jurassic seawater. *Geochimica et Cosmochimica Acta* 58, 1285–1301. [https://doi.org/10.1016/0016-7037\(94\)90382-4](https://doi.org/10.1016/0016-7037(94)90382-4)
- Jones, C.E., Jenkyns, H.C., Coe, A.L., Hesselbo, S.P., 1994b. Strontium isotopic variations in Jurassic and Cretaceous seawater. *Geochimica et Cosmochimica Acta* 58, 3061–3074. [https://doi.org/10.1016/0016-7037\(94\)90179-1](https://doi.org/10.1016/0016-7037(94)90179-1)
- Landrein, P., Vigneron, G., Delay, J., Lebon, P., Pagel, M., 2013. Lithologie, hydrodynamisme et thermicité dans le système sédimentaire multicouche recoupé par les forages Andra de Montiers-sur-Saulx (Meuse). *Bulletin de la Société Géologique de France* 184, 519–543. <https://doi.org/10.2113/gssgfbull.184.6.519>
- Lavastre, V., Ader, M., Buschaert, S., Petit, E., Javoy, M., 2011. Water circulation control on carbonate- $\delta^{18}\text{O}$  records in a low permeability clay formation and surrounding limestones: The Upper Dogger–Oxfordian sequence from the eastern Paris basin, France. *Applied Geochemistry* 26, 818–827. <https://doi.org/10.1016/j.apgeochem.2011.02.003>
- Lavastre, V., Le Gal La Salle, C., Michelot, J.-L., Giannesini, S., Benedetti, L., Lancelot, J., Lavielle, B., Massault, M., Thomas, B., Gilabert, E., Boulès, D., Clauer, N., Agrinier, P., 2010. Establishing constraints on groundwater ages with  $^{36}\text{Cl}$ ,  $^{14}\text{C}$ ,  $^3\text{H}$ , and noble gases: A case study in the eastern Paris basin, France. *Applied Geochemistry* 25, 123–142. <https://doi.org/10.1016/j.apgeochem.2009.10.006>
- Lavastre, V., Jendzejewski, N., Agrinier, P., Javoy, M., Evrard, M., 2005. Chlorine transfer out of a very low permeability clay sequence (Paris Basin, France):  $^{35}\text{Cl}$  and  $^{37}\text{Cl}$  evidence.



- 741        *Geochimica et Cosmochimica Acta* 69, 4949–4961.  
 742        <https://doi.org/10.1016/j.gca.2005.04.025>
- 743    Lefort, A., Lathuilière, B., Carpentier, C., Huault, V., 2011. Microfossil assemblages and relative  
 744        sea-level fluctuations in a lagoon at the Oxfordian/Kimmeridgian boundary (Upper  
 745        Jurassic) in the eastern part of the Paris Basin. *Facies* 57, 649–662.  
 746        <https://doi.org/10.1007/s10347-010-0259-4>
- 747    Lerouge, C., Gaucher, E.C., Tournassat, C., Negrel, P., Crouzet, C., Guerrot, C., Gautier, A.,  
 748        Michel, P., Vinsot, A., Buschaert, S., 2010. Strontium distribution and origins in a natural  
 749        clayey formation (Callovia-Oxfordian, Paris Basin, France): A new sequential extraction  
 750        procedure. *Geochimica et Cosmochimica Acta* 74, 2926–2942.  
 751        <https://doi.org/10.1016/j.gca.2010.02.013>
- 752    Maes, P., 2002. Circulations de fluides et interactions eau/roche passées et actuelles dans la  
 753        pile sédimentaire du site de Meuse/Haute-Marne: apport des isotopes du Sr et  
 754        conséquences (PhD Thesis), Université Montpellier, Montpellier (308 pp.).
- 755    Mangelot, X., Gasparrini, M., Gerdes, A., Bonifacie, M., Rouchon, V., 2018. An emerging  
 756        thermochronometer for carbonate-bearing rocks:  $\Delta 47$  (U-Pb). *Geology* 46, 1067–1070.  
 757        <https://doi.org/10.1130/G45196.1>
- 758    Mangelot, X., Gasparrini, M., Rouchon, V., Bonifacie, M., 2018. Basin-scale thermal and fluid  
 759        flow histories revealed by carbonate clumped isotopes ( $\Delta 47$ ) – Middle Jurassic  
 760        carbonates of the Paris Basin depocentre. *Sedimentology* 65, 123–150.  
 761        <https://doi.org/10.1111/sed.12427>
- 762    Matray, J.M., Lambert, M., Fontes, J.C., 1994. Stable isotope conservation and origin of saline  
 763        waters from the Middle Jurassic aquifer of the Paris Basin, France. *Applied*  
 764        *Geochemistry* 9, 297–309. [https://doi.org/10.1016/0883-2927\(94\)90040-X](https://doi.org/10.1016/0883-2927(94)90040-X)
- 765    Mazurek, M., 1999. Evolution of gas and aqueous fluid in low-permeability argillaceous rocks  
 766        during uplift and exhumation of the central Swiss Alps. *Applied Geochemistry* 15, 211–  
 767        234. [https://doi.org/10.1016/S0883-2927\(99\)00062-1](https://doi.org/10.1016/S0883-2927(99)00062-1)
- 768    Mazurek, M., Davis, D.W., Madritsch, H., Rufer, D., Villa, I.M., Sutcliffe, C.N., de Haller, A.,  
 769        Traber, D., 2018a. Veins in clay-rich aquitards as records of deformation and fluid-flow  
 770        events in northern Switzerland. *Applied Geochemistry* 95, 57–70.  
 771        <https://doi.org/10.1016/j.apgeochem.2018.05.010>
- 772    Moldovanyi, E.P., Walter, L.M., Brannon, J.C., Podosek, F.A., 1990. New constraints on  
 773        carbonate diagenesis from integrated Sr and S isotopic and rare earth element data,  
 774        Jurassic Smackover Formation, U.S. Gulf Coast. *Applied Geochemistry* 5, 449–470.  
 775        [https://doi.org/10.1016/0883-2927\(90\)90020-6](https://doi.org/10.1016/0883-2927(90)90020-6)
- 776    Montanari, D., Minissale, A., Doveri, M., Gola, G., Trumphy, E., Santilano, A., Manzella, A., 2017.  
 777        Geothermal resources within carbonate reservoirs in western Sicily (Italy): A review.  
 778        *Earth-Science Reviews* 169, 180–201. <https://doi.org/10.1016/j.earscirev.2017.04.016>
- 779    Muñoz-López, D., Alías, G., Cruset, D., Cantarero, I., Jonh, C.M., Travé, A., 2020. Influence of  
 780        basement rocks on fluid evolution during multiphase deformation: the example of the  
 781        Estamariu thrust in the Pyrenean Axial Zone. *Solid Earth*, 11, 2257–2281  
 782        <https://doi.org/10.5194/se-11-2257-2020>
- 783    Paganoni, M., Al Harthi, A., Morad, D., Morad, S., Ceriani, A., Mansurbeg, H., Al Suwaidi, A., Al-  
 784        Aasm, I.S., Ehrenberg, S.N., Sirat, M., 2016. Impact of stylolitization on diagenesis of a  
 785        Lower Cretaceous carbonate reservoir from a giant oilfield, Abu Dhabi, United Arab  
 786        Emirates. *Sedimentary Geology* 335, 70–92.  
 787        <https://doi.org/10.1016/j.sedgeo.2016.02.004>
- 788    Pagel, M., Bonifacie, M., Schneider, D.A., Gautheron, C., Brigaud, B., Calmels, D., Cros, A.,  
 789        Saint-Bezar, B., Landrein, P., Sutcliffe, C., Davis, D., Chaduteau, C., 2018. Improving  
 790        paleohydrological and diagenetic reconstructions in calcite veins and breccia of a  
 791        sedimentary basin by combining  $\Delta 47$  temperature,  $\delta 18\text{O}_{\text{water}}$  and U-Pb age. *Chemical*

- Geology 481, 1–17. <https://doi.org/10.1016/j.chemgeo.2017.12.026>
- Pin, C., Joannon, S., Bosq, C., Le Fèvre, B., Gauthier, P.-J., 2003. Precise determination of Rb, Sr, Ba, and Pb in geological materials by isotope dilution and ICP-quadrupole mass spectrometry following selective separation of the analytes. *Journal of Analytical Atomic Spectrometry* 8, 135–141. <https://doi.org/10.1039/B211832G>
- Pisapia, C., Deschamps, P., Battani, A., Buschaert, S., Guihou, A., Hamelin, B., Brulhet, J., 2018. U/Pb dating of geodic calcite: new insights on Western Europe major tectonic events and associated diagenetic fluids. *Journal of the Geological Society* 175, 60–70. <https://doi.org/10.1144/jgs2017-067>
- Pourcelot, L., Stille, P., Aubert, D., Solovitch-Vella, N., Gauthier-Lafaye, F., 2008. Comparative behaviour of recently deposited radiostrontium and atmospheric common strontium in soils (Vosges mountains, France). *Applied Geochemistry* 23, 2880–2887. <https://doi.org/10.1016/j.apgeochem.2008.04.013>
- Prosser, D.J., Daws, J.A., Fallick, A.E., Williams, B.P.J., 1993. Geochemistry and diagenesis of stratabound calcite cement layers within the Rannoch Formation of the Brent Group, Murchison Field, North Viking Graben (northern North Sea). *Sedimentary Geology* 87, 139–164. [https://doi.org/10.1016/0037-0738\(93\)90002-M](https://doi.org/10.1016/0037-0738(93)90002-M)
- Rebeix, R., Le Gal La Salle, C., Michelot, J.-L., Verdoux, P., Noret, A., Monvoisin, G., Ganesinni, S., Lancelot, J., Simler, R., 2011. Tracing the origin of water and solute transfers in deep groundwater from Oxfordian, Dogger and Trias formations in the East of the Paris Basin – France. *Physics and Chemistry of the Earth, Parts A/B/C* 36, 1496–1510. <https://doi.org/10.1016/j.pce.2011.07.015>
- Sandström, B., Tullborg, E.-L., 2009. Episodic fluid migration in the Fennoscandian Shield recorded by stable isotopes, rare earth elements and fluid inclusions in fracture minerals at Forsmark, Sweden. *Chemical Geology* 266, 126–142. <https://doi.org/10.1016/j.chemgeo.2009.04.019>
- Sutcliffe, C.N., Thibodeau, A.M., Davis, D.W., Al-Aasm, I., Parmenter, A., Zajacz, Z., Jensen, M., 2020. Hydrochronology of a proposed deep geological repository for low- and intermediate-level nuclear waste in southern Ontario from U–Pb dating of secondary minerals: response to Alleghanian events. *Canadian Journal of Earth Sciences* 57, 494–505. <https://doi.org/10.1139/cjes-2019-0005>
- Swart, P.K., 2015. The geochemistry of carbonate diagenesis: The past, present and future. *Sedimentology* 62, 1233–1304. <https://doi.org/10.1111/sed.12205>
- Vincent, B., Emmanuel, L., Houel, P., Loreau, J.-P., 2007. Geodynamic control on carbonate diagenesis: Petrographic and isotopic investigation of the Upper Jurassic formations of the Paris Basin (France). *Sedimentary Geology* 197, 267–289. <https://doi.org/10.1016/j.sedgeo.2006.10.008>
- Vinsot, A., Mettler, S., Wechner, S., 2008. In situ characterisation of the Callovo-Oxfordian pore water composition. *Physics and Chemistry of the Earth, Parts A/B/C* 33, S75–S86. <https://doi.org/10.1016/j.pce.2008.10.048>
- Wallin, B., Peterman, Z., 2015. Compilation and Review of  $^{87}\text{Sr}/^{86}\text{Sr}$  and Stable Isotopes from Groundwater, Calcite Fracture Fillings, Mineral, and Whole-Rock Sampling at Äspö, Sweden. *Groundwater* 53, 103–112. <https://doi.org/10.1111/gwat.12173>
- Worden, R.H., Matray, J.-M., 1995. Cross formational flow in the Paris Basin. *Basin Research* 7, 53–66. <https://doi.org/10.1111/j.1365-2117.1995.tb00095.x>
- Zhu, D., Liu, Q., Zhang, J., Ding, Q., He, Z., Zhang, X., 2019. Types of Fluid Alteration and Developing Mechanism of Deep Marine Carbonate Reservoirs. *Geofluids* 2019, 1–18. <https://doi.org/10.1155/2019/3630915>



**Declaration of interests**

☒ The authors declare that they have no known competing financial interests or personal relationships that could have appeared to influence the work reported in this paper.

☐ The authors declare the following financial interests/personal relationships which may be considered as potential competing interests:

--